



Ranking of tree-ring based hydroclimate reconstructions of the past millennium

Fredrik Charpentier Ljungqvist^{a, b, c, *}, Alma Piermattei^d, Andrea Seim^e, Paul J. Krusic^{d, f}, Ulf Büntgen^{d, g, h, i}, Minhui He^j, Alexander V. Kirdyanov^{d, k, l}, Jürg Luterbacher^{m, n}, Lea Schneider^m, Kristina Seftigen^{o, p, g}, David W. Stahle^q, Ricardo Villalba^r, Bao Yang^s, Jan Esper^t

^a Department of History, Stockholm University, Stockholm, Sweden

^b Bolin Centre for Climate Research, Stockholm University, Stockholm, Sweden

^c Swedish Collegium for Advanced Study, Uppsala, Sweden

^d Department of Geography, University of Cambridge, Cambridge, United Kingdom

^e Chair of Forest Growth, Institute of Forest Sciences, Albert Ludwig University of Freiburg, Freiburg, Germany

^f Department of Physical Geography, Stockholm University, Stockholm, Sweden

^g Dendro Sciences Group, Swiss Federal Research Institute WSL, Birmensdorf, Switzerland

^h CzechGlobe Global Change Research Institute CAS, Brno, Czech Republic

ⁱ Department of Geography, Faculty of Science, Masaryk University, Brno, Czech Republic

^j Center for Ecological Forecasting and Global Change, College of Forestry, Northwest Agriculture and Forestry University, Yangling, China

^k Sukachev Institute of Forest SB RAS, Akademgorodok, Krasnoyarsk, Russia

^l Institute of Ecology and Geography, Siberian Federal University, Krasnoyarsk, Russia

^m Department of Geography, Climatology, Climate Dynamics and Climate Change, Justus Liebig University, Giessen, Germany

ⁿ Centre for International Development and Environmental Research, Justus Liebig University, Giessen, Germany

^o Regional Climate Group, Department of Earth Sciences, University of Gothenburg, Gothenburg, Sweden

^p Georges Lemaître Centre for Earth and Climate Research, Université Catholique de Louvain, Louvain-la-Neuve, Belgium

^q Department of Geosciences, University of Arkansas, Fayetteville, United States

^r Instituto Argentino de Nivología, Glaciología y Ciencias Ambientales IANIGLA, CCT-CONICET-Mendoza, Mendoza, Argentina

^s Key Laboratory of Desert and Desertification, Northwest Institute of Eco-Environment and Resources, Chinese Academy of Sciences, Lanzhou, China

^t Department of Geography, Johannes Gutenberg University, Mainz, Germany

ARTICLE INFO

Article history:

Received 21 August 2019

Received in revised form

12 November 2019

Accepted 13 November 2019

Available online xxx

Keywords:

Paleoclimate

Dendrochronology

Dendroclimatology

Hydroclimate

Proxy data

Past millennium

Climate change

ABSTRACT

To place recent hydroclimate changes, including drought occurrences, in a long-term historical context, tree-ring records serve as an important natural archive. Here, we evaluate 46 millennium-long tree-ring based hydroclimate reconstructions for their *Data Homogeneity*, *Sample Replication*, *Growth Coherence*, *Chronology Development*, and *Climate Signal* based on criteria published by Esper et al. (2016) to assess tree-ring based temperature reconstructions. The compilation of 46 individually calibrated site reconstructions includes 37 different tree species and stem from North America ($n = 29$), Asia ($n = 10$); Europe ($n = 5$), northern Africa ($n = 1$) and southern South America ($n = 1$). For each criterion, the individual reconstructions were ranked in four groups, and results showed that no reconstruction scores highest or lowest for all analyzed parameters. We find no geographical differences in the overall ranking, but reconstructions from arid and semi-arid environments tend to score highest. A strong and stable hydroclimate signal is found to be of greater importance than a long calibration period. The most challenging trade-off identified is between high continuous sample replications, as well as a well-mixed age class distribution over time, and a good internal growth coherence. Unlike temperature reconstructions, a high proportion of the hydroclimate reconstructions are produced using individual series detrending methods removing centennial-scale variability. By providing a quantitative and objective evaluation of all available tree-ring based hydroclimate reconstructions we hope to boost future improvements in the development of such records and provide practical guidance to secondary users of these reconstructions.

© 2019 The Authors. Published by Elsevier Ltd. This is an open access article under the CC BY license (<http://creativecommons.org/licenses/by/4.0/>).

* Corresponding author. Department of History, Stockholm University, SE-106 91, Stockholm, Sweden.

E-mail address: fredrik.c.l@historia.su.se (F.C. Ljungqvist).

1. Introduction

Tree-ring chronologies built from living and dead trees offer a valuable source of information for understanding different aspects of natural and human history, ranging from archeological dating to past climate conditions. Tree-ring chronologies are both annually resolved and precisely dated (Douglass, 1909, 1920, 1928; 1941; Stokes and Smiley, 1968; Fritts, 1976; Schweingruber, 1988; Speer, 2010; Anchukaitis, 2017; Büntgen et al., 2018). Long chronologies can be developed in most temperate and subtropical areas of the world across almost all types of habitats (St George, 2014; St George and Ault, 2014). The availability of numerous tree-ring data sets from different sites and tree species, from diverse natural environments, allows for comprehensive statistical analyses (e.g., Björklund et al., 2017; Seftigen et al., 2018; Babst et al., 2019; Büntgen et al., 2019).

Depending on the dominant growth-limiting climate factor in a particular site, tree-ring data can be used to reconstruct either growing season temperature or hydroclimate variability (Fritts, 1976). Millennium-long temperature reconstructions, entirely or partly derived from tree-ring data, have gained the widest attention through their almost iconic status in the current global warming discourse (see, e.g., Frank et al., 2010; Masson-Delmotte et al., 2013; Smerdon and Pollack, 2016; Esper et al., 2018). Tree-ring based hydroclimate reconstructions are perhaps less widely known, but they play an equally important role in contributing to our understanding of climate variability over the past one to two millennia. The use of tree-ring data to understand past hydroclimate variability has also a considerably longer history than the use of tree-ring data to address temperature variability, as the science of dendrochronology was developed in the moisture-limited growth environment of the southwestern United States (Douglass, 1929, 1941). Notable earlier works in the field include Bogue (1905), Douglass (1917), Hawley and Clark (1940), Schulman (1956), and Fritts (1976). Some of the earliest examples of long calibrated precipitation, drought and streamflow reconstructions can be found in Schulman (1945), Meko et al. (1980), Cook and Jacoby (1983).

Reconstructing hydroclimate is more challenging than reconstructing temperature as precipitation and drought are highly affected by topography and local features (Feng et al., 2013) and have greater spatial variability (Osborn and Hulme, 1997; Datta et al., 2003; Hofstra and New, 2009; Büntgen et al., 2010a,b; Wan et al., 2013). Precipitation shows significant spatial correlations of ~500–700 km at decadal time-scales (Cook et al., 2004; Ljungqvist et al., 2016; Schneider et al., 2019) compared to up to several thousand kilometers for temperature (Jones et al., 1997; Christiansen and Ljungqvist, 2017).

Despite these challenges several large-scale gridded hydroclimate reconstructions, covering major portions of continents, have been produced using tree-ring data: e.g. the North American Drought Atlas (Cook et al., 2004), the Monsoon Asia Drought Atlas (Cook et al., 2010), the Old World Drought Atlas (Cook et al., 2015a, b), the Mexican Drought Atlas (Stahle et al., 2016), the Eastern Australia and New Zealand Drought Atlas (Palmer et al., 2015) and recently the combined Global Drought Atlas (Marvell et al., 2019) covering large portions of the world back to 1400 CE and offering reasonable coverage for parts of the Northern Hemisphere back to 1000 CE. However, the majority of tree-ring chronologies included in these gridded reconstructions have not been published as individual quality-assessed hydroclimate reconstructions. Although the chronologies in the drought atlases,

when used together, provide a skillful drought reconstruction over space and time, their strength lies in the representation of the general hydroclimatic condition in a region due to the applied aggregation, and thus interpolation, approach. Complementary to those drought atlases, however, it is important to use individual tree-ring based site reconstructions to understand the underlying data and investigate local hydroclimatic conditions. This is of paramount importance especially when the local hydroclimate–tree growth relationship deviates in season or in hydroclimatic metric from the one used in the drought atlases.

The network of millennium-long hydroclimate tree-ring based reconstructions is geographically confined to a few regions (Fig. 1) with the largest concentration in the southwestern United States, and a smaller cluster on the edge of the northeastern Tibetan Plateau. Considering the drought change difference between 1983–2016 and 1950–1982, one finds hydroclimate reconstructions distributed over both regions that tend to get wetter and regions that tend to get drier (Fig. 1). It is obvious that the present network of millennium-long reconstructions is woefully inadequate for capturing the spatially heterogeneous nature of hydroclimate variability.

1.1. Objectives

Future hydroclimate changes are arguably the largest uncertainty connected with global warming that, at the same time, likely have the largest environmental and societal impacts (Field et al., 2014; Schewe et al., 2014; Lehner et al., 2017; Trnka et al., 2018). State-of-the-art climate model simulations provide highly uncertain projections of hydroclimate changes at regional to continental scales (Stephens et al., 2010; Orłowsky and Seneviratne, 2013; Christensen et al., 2014; Nasrollahi et al., 2015). Climate model evaluation through paleoclimate reconstruction–simulation comparison studies is thus of utmost importance to improve the models' skill (e.g., Ault et al., 2013, 2014; Coats et al., 2015; Cook et al., 2015a, b, 2016; Smerdon et al., 2015; Ljungqvist et al., 2016, 2019; Xoplaki et al., 2016, 2018; Seftigen et al., 2017; Bothe et al., 2019). Hydroclimate reconstructions are therefore highly important for a deeper understanding of past, present and future hydroclimatic conditions and it is critically important to objectively assess and communicate the strengths and weaknesses of each individual record.

In this article, we evaluate and rank 46 millennium-long tree-ring based hydroclimate reconstructions by considering their *Data Homogeneity*, *Sample Replication*, *Growth Coherence*, *Chronology Development*, and *Climate Signal* using an ordinal scoring scheme set forth in Esper et al. (2016) for ranking tree-ring based temperature reconstructions. We discuss the implications of the ranking, provide recommendations for how to select hydroclimate reconstructions to use for different purposes, and make recommendations for the development of new hydroclimate reconstructions. In addition, we compare the results of the two rankings of hydroclimate and temperature reconstructions.

1.2. Reconstructed hydroclimatic metrics

Our compilation of tree-ring based hydroclimate reconstructions, extending back to 1000 CE, includes 24 reconstructions of precipitation, 11 reconstructions of streamflow, 6 reconstructions of the Palmer Drought Severity Index (PDSI; Palmer, 1965; van der Schrier et al., 2011), 3 reconstructions of

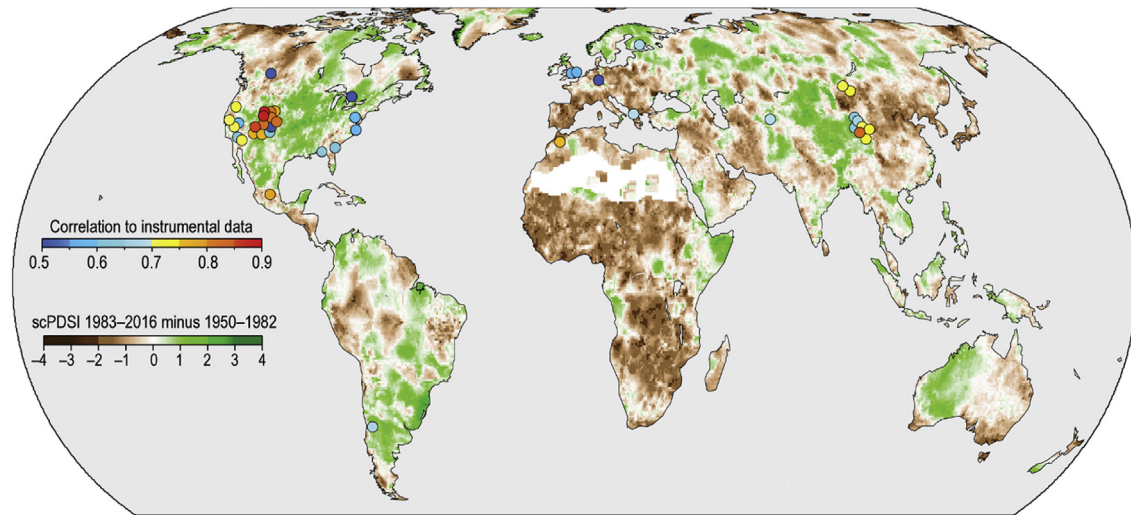


Fig. 1. Map of the locations of the 46 calibrated millennium-long hydroclimate tree-ring based reconstructions as filled circles showing the instrumental correlation values superimposed on annual mean scPDSI (van der Schrier et al., 2011) values of the period 1983–2016 minus the period 1950–1982.

moisture availability/balance, 1 reconstruction of the Standardized Precipitation Index (SPI; McKee et al., 1993), and 1 reconstruction of Palmer Hydrological Drought Index (PHDI) (Karl, 1986). Precipitation is the most easily available metric as it is directly derived from meteorological station data, although it does not fully reflect the complex hydrological systems. Furthermore, tree-ring hydroclimate sensitivity might vary depending on soil characteristics and evapotranspiration rates, making different drought metrics more or less suitable.

PDSI integrates precipitation and temperature to estimate relative dryness ranging from -10 (very dry) to $+10$ (very wet) (Palmer, 1965; Dai et al., 2004; Wells et al., 2004; van der Schrier et al., 2011). It tracks long-term changes in physiological drought, relative to the mean conditions in a given region, as it combines a physical water balance model with temperature and thus considers potential evapotranspiration (Hobbins et al., 2008). PHDI captures the slower impacts of drought and was developed to quantify long-term hydrological effects better than the PDSI (Jacobi et al., 2013).

SPI quantifies the observed precipitation as a standardized departure from the long-term mean (Keyantash and Dracup, 2002). One potential weakness with SPI is that it does not consider changes in evapotranspiration since it only reflects changes in water supply. The metric relates well to soil moisture on shorter timescales and to groundwater and reservoir storage on longer timescales (McKee et al., 1993). It is typically a more comparable metric across regions than PDSI, albeit this limitation of PDSI is greatly relieved in self-calibrated PDSI variant (scPDSI; Wells et al., 2004; van der Schrier et al., 2011).

Streamflow can be reconstructed from tree-ring data, as both river discharge and tree growth could be modulated by common precipitation and evaporation patterns at a local to regional scale (Schulman, 1945; Stockton, 1975; Stockton and Jacoby, 1976; Woodhouse et al., 2006; Ho et al., 2016). However, streamflow has its own characteristics: after a heavy precipitation, discharge typically reaches a peak, and then gradually subsides to base flow.

2. Materials and methods

2.1. Tree-ring based hydroclimate reconstructions

A literature review (completed in February 2019) resulted in the identification of 48 tree-ring width based hydroclimate reconstructions extending back to at least 1000 CE, each with a minimum replication in any given year of at least three measurement series. Only 46 of these 48 reconstructions are included in this assessment since the raw data and sufficient information from two reconstructions – the Northeastern Tibetan Plateau precipitation reconstruction by Liu et al. (2006) and the Qaidam Basin moisture availability reconstruction by Yin et al. (2008) – could not be obtained. All data used here were otherwise either accessible from public repositories or made available to us by the original authors. We did not include older reconstructions using mainly the same tree-ring material as in a newer version.¹ Moreover, all tree-ring isotope based reconstructions (see e.g., Duffy et al., 2019) were excluded from this assessment as they either lack annual resolution (e.g., Edwards et al., 2008, 2017; Wang et al., 2013; Kress et al., 2014) or the reconstruction was derived from annually pooled samples (e.g., Treydte et al., 2006; Griesinger et al., 2017), precluding the calculation of key metrics used in this assessment.

Out of the 46 tree-ring width based hydroclimate reconstructions, 10 are from Asia, 5 from Europe, 1 from (northern) Africa, 29 from North America, and 1 from (southern) South America. The five reconstructions from Europe and the one from (northern) Africa are treated as one group (Fig. 1; Table 1). The 46 reconstructions are derived from 37 tree species representing 16 different genera, with *Pinus* ($n = 21$), *Pseudotsuga* ($n = 14$), and *Juniperus* ($n = 11$) being the most common. Most species ($n = 22$), however, occur only in one single reconstruction. The majority of the reconstructions ($n = 29$) are composed of one tree species, but 11 include two species, and six combine three or more species (Table 1). Only seven reconstructions are composed of ring width data solely from living trees, mainly from China, while 39

¹ For example, the Heihe River, China, streamflow reconstruction by Qin et al. (2010) is superseded by that in Yang et al. (2012).

Table 1
List of all the 46 tree-ring reconstructions, extending back at least to 1000 CE, published as calibrated hydroclimate reconstructions. The abbreviation code for tree species follows the standard used in the International Tree-Ring Data Bank (ITRDB; [Grissino-Mayer and Fritts, 1997](#)) as listed in [Grissino-Mayer \(1993\)](#). Abbreviations: EW = earlywood; LW = latewood.

Reconstruction	Reference	Long.	Lat.	Species	Signal	Season
1. Albemarle Sound, USA (EW)	Stahle et al. (2013)	−76.00	36.00	TADI	PHDI	July
2. A'nyemaqen, China	Gou et al. (2010)	99.50	34.50	JUPR	Streamflow	August–July
3. Atlas Mountains, Morocco	Esper et al. (2007)	−5.07	33.02	COAL	PDSI	February–June
4. Barranca de Amealco, Mexico	Stahle et al. (2011)	−100.07	20.21	TACU	PDSI	June
5. Bear River, USA	DeRose et al. (2015)	−110.85	40.97	JUOS	Streamflow	October –September
6. Central Chile	Garreaud et al. (2017)	−70.34	−34.35	AUCH	Precipitation	June–December
7. Central Europe	Büntgen et al. (2011)	9.00	50.00	QUSP	Precipitation	
8. Choctawhatchee River, USA (EW)	Stahle et al. (2012)	−85.88	30.47	TADI	Precipitation	April–May
9. Choctawhatchee River, USA (LW)	Stahle et al. (2012)	−85.88	30.47	TADI	Precipitation	June–July
10. Colorado River, USA	MacDonald et al. (2008)	−114.50	33.50	PIAR, PILO, PIFL, LALY, PSME	Streamflow	October –September
11. Delingha, China	Shao et al. (2005)	97.80	37.10	JUPR	Precipitation	July–June
12. Dulan, China	Sheppard et al. (2004)	99.00	37.00	SBPI	Precipitation	July–June
13. East Anglia, UK	Cooper et al. (2013)	1.00	52.50	QUPE, QURO	Precipitation	March–July
14. El Malpais, USA	Grissino-Mayer (1995)	−108.18	34.97	PSME, PIPO	Precipitation	July–July
15. El Malpais, USA (EW)	Stahle et al. (2009)	−108.18	34.97	PSME, PIPO	Precipitation	September–May
16. El Malpais, USA (LW)	Stahle et al. (2009)	−108.18	34.97	PSME, PIPO	Precipitation	June–July
17. Flowerpot, Canada	Buckley et al. (2004)	−81.50	45.10	THOC	Precipitation	June–July
18. Georgia, USA	Stahle and Cleaveland (1992)	−81.80	31.62	TADI	Precipitation	March–July
19. Heihe River Basin, China	Yang et al. (2012)	100.00	38.20	SBPI	Streamflow	August–July
20. Hexi Corridor, China	Yang et al. (2019)	98.03	39.55	JUPR	scPDSI	May–June
21. Jemez Mountains, USA	Touchan et al. (2011)	−106.50	36.00	PSME, PISF, PIPO	Precipitation	October–June
22. Khorgo, Mongolia	Hessl et al. (2018)	99.87	48.17	PISI	PDSI	June–September
23. Lee Ferry, USA	Meko et al. (2007)	−111.58	36.85	PSME, PIED	Streamflow	
24. Little Snake River, USA	Gray et al. (2011)	−107.75	40.75	PSME, PIMO	Streamflow	October –September September–May
25. Mesa Verde, USA	Stahle et al. (2015)	−108.48	37.18	PSME	Moisture balance	
26. Mesa Verde, USA	Stahle et al. (2015)	−108.48	37.18	PSME	Moisture balance	June–July
27. Mount San Gorgonio, USA	MacDonald (2007)	−116.80	34.12	PIJE	PDSI	January–April
28. Mount Smolikas, Greece	Klippel et al. (2018)	20.75	40.25	PIHE	SPI	June–July
29. Northeastern Tibetan Plateau, China	Yang et al. (2014)	98.00	37.00	JUPR	Precipitation	July–June
30. Pamir–Alay Mountains, Tajikistan	Opała-Owczarek and Niedźwiedź (2018)	69.00	39.00	JUSM	Precipitation	December –February
31. Potomac River, USA	Maxwell et al. (2011)	−77.53	39.27	CYOV, JUVI, LITU, MAAC, PCRU, QUAL, QUPR, TADI, TSCA	Streamflow	May–September
32. Qilian Mountains, China	Zhang et al. (2011)	99.50	38.50	JUPR	Precipitation	August–July
33. Sacramento River, USA	MacDonald et al. (2008)	−121.63	38.70	PILO, PIFL, JUOC	Streamflow	
34. Southern Colorado Plateau, USA	Salzer and Kipfmüller (2005)	−111.40	35.20	PSME, PIED	Precipitation	October–July
35. Southern Finland	Helama et al. (2009)	28.50	61.50	PISY	Precipitation	May–June
36. Southern Sierra Nevada, USA	Graumlich (1993)	−118.90	36.90	JUOC	Precipitation	December –February
37. Southerncentral England, UK	Wilson et al. (2013)	−1.50	52.00	QUPE, QURO	Precipitation	March–July
38. Summitville, USA	Routson et al. (2011)	−106.59	37.43	PIAR	Precipitation	March–July
39. Tavaputs Plateau, USA	Knight et al. (2010)	−110.40	39.70	PSME	Precipitation	July–July
40. Upper Arkansas River Basin, USA	Woodhouse et al. (2011)	−106.00	38.50	PSME, PIPO, PIED	Moisture availability	October –September
41. Upper Klamath River Basin, USA	Malevich et al. (2013)	−121.78	42.20	JUOC, PIPO, PIJE, QUDG	Precipitation	October –September
42. Uurgat, Mongolia	Hessl et al. (2018)	101.77	46.68	PISI	PDSI	June–September
43. Whirlpool point, Canada	Case and MacDonald (2003)	−116.45	52.00	PIFL, PCMA	Streamflow	October –September
44. White Mountains, USA	Hughes and Graumlich (1996)	−118.17	37.45	PILO	Precipitation	July–June
45. White River, USA	Gray et al. (2011)	−108.00	40.00	PSME, PIMO	Streamflow	October –September
46. Yampa River, USA	Gray et al. (2011)	−108.33	40.48	PSME, PIMO	Streamflow	October –September

are composed of living trees in combination with relict material from archeological, historical, remnant, and/or sub-fossil samples. The season of the strongest tree-growth response to hydroclimate differs among the reconstructions (see column “Season” in [Table 1](#)).

2.2. Hydroclimate tree-ring chronology characteristics and metrics

The characteristics *Data Homogeneity*, *Sample Replication*, *Growth Coherence*, *Chronology Development*, and *Climate Signal* described in [Esper et al. \(2016\)](#) are here adapted for hydroclimate

reconstructions (sections 2.3.1 to 2.3.5). In most instances, information about *Data Homogeneity* and *Climate Signal* were obtained from the original publications. For the remaining characteristics, each value was calculated using the program ARSTAN (version ARS41d_xp) (Cook and Krusic, 2005). Each characteristic (see sections 2.3.1 to 2.3.5) is used to produce an ordinal scoring scheme to rank the 46 tree-ring hydroclimate reconstructions. The scores for each criterion and their combination are divided into four classes (from highest to lowest rank): class A, class B, class C, and class D. In the quantitative ranking of *Sample Replication*, *Growth Coherence*, *Chronology Development*, and *Climate Signal*, the 12 top-ranked hydroclimate reconstructions fall in class A, ranks 13–24 in class B, ranks 25–35 in class C, and ranks 36–46 in class D. In the mainly qualitative ranking of the *Data Homogeneity* an uneven number of reconstructions fall into the four hierarchical classes (11 reconstructions in class A, 14 class B, 14 class C, and 7 class D). To produce an overall score, the individual ranking order for each characteristic (sections 2.3.1 to 2.3.5) is combined.

2.2.1. Data homogeneity

The category *Data Homogeneity* combines characteristics of the (i) “Source” of tree-ring samples, (ii) “Type of chronology”, (iii) “Number” of tree species, (iv) “Temporal clustering” of tree-ring data, and (v) more general “Remarks” on the sampling site(s). *Source* includes information about the origin of tree-ring samples, the number of sampling sites, and their location in relation to each other. The *Data Homogeneity* score takes into account whether, and to what extent, the tree-ring samples originate from one or more sites. This information was obtained either from the original publication or via personal communication with the author(s)/data contributor(s). *Chronology type* differentiates between two types of tree-ring reconstructions: composite “C” reconstructions, composed of living in addition to relict (*historical/remnant/sub-fossil*) material, and living “L” reconstructions composed only of samples from living trees. *Historic* denotes samples from both archeological excavations and standing structures. *Remnant* denotes samples from dead wood found on the ground in different states of conservation. *Sub-fossil* denotes samples retrieved from sediments. *Number of Species* considers the number of different tree species contributing to a reconstruction. *Temporal clustering* refers to when the contribution of tree-ring data from distinct homogeneous sites and/or a specific tree species dominate specific periods of the past millennium. Such clustering can complicate the preservation of low-frequency climate information (*sensu*, Melvin et al., 2013). *Remark* summarizes particular features of the data in a particular reconstruction relevant to the *Data Homogeneity* score.

2.2.2. Sample replication

The availability of tree-ring series varies over time, resulting in an uneven temporal distribution over the past millennium with typically increasingly fewer series back in time. We consider how these temporal changes affect reconstruction skill in the *Sample Replication* metric by integrating information about (i) “Mean replication”, (ii) “Maximum replication”, (iii) “Minimum replication”, and (iv) “11th/20th Century Ratio”. *Mean Replication* denotes the average number of measurement series (either core samples or radii from disks) considering all years from 1000 CE to the most recent year of a reconstruction (thus, meaning that the exact number of years can differ slightly due to the different end dates of the reconstructions). *Maximum Replication* and *Minimum Replication* refer to the maximum and minimum numbers of contributing measurements at any year in the reconstruction. The *11th/20th Century Ratio* refers to the mean 11th century replication divided by the mean 20th century replication multiplied by 100. This metric is particularly important since tree-ring based reconstructions are

calibrated over the typically well-replicated recent period. We calculate the combined *Sample Replication* score by summing the first three values (i + ii + iii) and multiplying the result by (iv). As explained in Esper et al. (2016), these measures – as well as those for the other scores described below – are somewhat arbitrary but derived through dendroclimatological expert knowledge to produce an ordinal scoring system that permits the comparison and ranking of tree-ring based reconstructions. *Sample Replication* was calculated using the program ARSTAN.²

2.2.3. Growth coherence

Growth coherence is expressed by the correlation between the individual measurement series: the so-called inter-series correlation (Rbar) (Wigley et al., 1984). *Growth Coherence* is an important chronology characteristic when evaluating the temporal reliability of a tree-ring based climate reconstruction. Using the program ARSTAN, we calculated the running mean Rbar value for every 10 years of a chronology using a 100-year window with an overlap of 90 years from 1000 CE onwards. The final *Growth Coherence* score is obtained by summing the (i) mean Rbar, (ii) maximum Rbar, and (iii) minimum Rbar and multiplying the resulting sum by the (iv) 11th/20th century ratio Rbar (in %). The mean, as well as the minimum and maximum Rbar were calculated in a similar manner from 1050 CE onwards. In order to avoid biased positive results from very high Rbar values in the 11th century compared to in the 20th century, the maximum allowed Rbar ratio is capped at 150% in the calculation of the final *Growth Coherence* score. This 150% ceiling only affects three reconstructions, all from the United States: Potomac River (Maxwell et al., 2011), Southern Sierra Nevada (Graumlich, 1993), and Upper Arkansas River Basin (Woodhouse et al., 2011).

2.2.4. Chronology development

The *Chronology Development* score incorporates four metrics: (i) type of detrending (“1” for Regional Curve Standardization (RCS), and “2” for individual-series detrending method), (ii) the square root of the difference between the maximum and the minimum age, (iii) the slope of the linear regression in the age curve multiplied by 100, and (iv) the maximum retained low-frequency score (“1” for multi-centennial and “2” for decadal to centennial). The choice of detrending method to remove tree-age related growth trends from the raw measurement series can have profound effect on the ability to preserve low-frequency variability and long-term trends in tree-ring reconstructions. Only certain detrending methods can overcome limitations induced by the segment length of individual tree-ring series (Cook et al., 1995). The RCS method (Briffa et al., 1992; Esper et al., 2003) is most commonly used to achieve trend preservation and the maximum retained low-frequency score is “1” for RCS detrended. Reconstructions produced by individual series detrending are by default supposed not to preserve low-frequency variability beyond their segment length and obtain the score “2”. However, chronologies with tree-ring series, on average, exceeding 400 years are still supposed to retain some multi-centennial variability. We calculated the difference between the maximum and minimum age over the past millennium, and the slope of the linear regression fit to the age curve. In the ranking of temperature reconstructions by Esper et al. (2016), the maximum low-frequency information a reconstruction is arguably able to retain is divided into three categories: multi-centennial = “1”, to centennial = “2”, to decadal = “3”. Here, for our

² The 11th century sample depth is calculated over the period 1001 to 1100, and the 20th century sample depth is calculated from 1901 to the most recent year of a reconstruction.

ranking, we only use two categories: multi-centennial = “1” and decadal to centennial = “2”. The rationale for a two-category scale when working with hydroclimate reconstructions is because, compared to temperature, it is less certain what are the deterministic and stochastic controls on hydroclimate low-frequency variability (Hurst, 1951; Pelletier and Turcotte, 1997; Markonis and Koutsoyiannis, 2016). The final *Chronology Development* score is obtained by multiplying (i) the method score (“1” for RCS, “2” for individual detrending), with (ii) the square root of the maximum–minimum age difference, (iii) the absolute linear regression slope multiplied by 100, and (iv) the maximum retained low-frequency score.

2.2.5. Climate signal

We acknowledge the limitations with the *Climate Signal* metric considering that the assessment of hydroclimate signal strength to a large degree is dependent on the quality and length of the instrumental data. Moreover, in some cases, especially in regions with a short and sparse network of instrumental data, the hydroclimate signal in the trees may in fact be better than the instrumental data used for calibration. The *Climate Signal* score is derived by (i) calculating the square root of the number of years of overlap between the reconstruction and the instrumental target used for calibration, multiplied by the residual between, (ii) the correlation coefficients between tree-ring chronologies and instrumental climate data, and (iii) the difference between correlation values of the calibration/verification periods. When the calibration/verification statistics are not reported, we estimate the difference based on our calculations using gridded instrumental data. In addition, we included another variable (iv) to account for a calibration period that was deliberately shortened to avoid “divergence”, i.e., an anomalous offset between tree growth and climate sensitivity (*sensu* D’Arrigo et al., 2008). When such “divergence” is reported in the original publication, and the calibration period has been truncated, we use 0.5 as a multiplier instead of 1 as in all other cases. The final *Climate Signal* score is obtained by calculating the square root $i \times (ii - iii) \times iv$.

3. Results

3.1. Detailed tree-ring chronology rankings

3.1.1. Data homogeneity

The reconstructions scoring the highest (rank A) by *Data Homogeneity* (Table 3), of which none are from Europe, are derived from only one site or, in case of the Tavaputs Plateau (Knight et al., 2010), from two very nearby sites in one canyon. Moreover, when the reconstructions are only based on one tree species, and when the data are from only one site, it is not possible for temporal clustering to occur. The reconstructions scoring second highest (class B) are based on tree-ring material from either one or two or several sites (e.g., Barranca de Amealco; Stahle et al., 2011 and Flowerpot; Buckley et al., 2004). In cases when they are based on only one site this site includes less homogeneous material than those in class A. When the data are from two or more sites, these are typically homogeneous growth environments in close proximity and the reconstructions are composed of at most two species. There may exist inhomogeneities such as early chronology portions that are based on only one site (e.g., Atlas Mountains; Esper et al., 2007), substantial changes in mean ring width level (e.g., Barranca de Amealco; Stahle et al., 2011), data obtained from two different river systems (e.g., Choctawhatchee River; Stahle et al., 2012), different microsite conditions (e.g., Flowerpot; Buckley et al., 2004).

Reconstructions scoring less well (class C) typically consist of

rather inhomogeneous material, often collected across a large region. In some cases, the data are from a larger number of sites (e.g., 17 living tree sites and 5 archeological sites on the Northeastern Tibetan Plateau; Yang et al., 2014). Parts of the chronologies may also be derived from historical and/or archeological wood that does not necessarily provenance from the same area or environment as the living or remnant samples in the same chronology (e.g., Central Europe; Büntgen et al., 2011, Dulan; Sheppard et al., 2004, East Anglia; Cooper et al., 2013, Southeastern England; Wilson et al., 2013, and Mesa Verde; Stahle et al., 2015). The reconstructions scoring lowest in *Data Homogeneity* (class D) do not necessarily consist of more sites than those in class C. However, the sites are geographically more dispersed as well as diverse in their growth environments. All reconstructions in class D, except one, include three to up to nine different tree species (see Table 2). All class D reconstructions are from North America, including many that consist of numerous sites, widely dispersed over several states, and separated by distances up to several hundreds of kilometers. It is thus the number of sites, plus the distance between them, as well as the inhomogeneous growth environments that primarily are impacting *Data Homogeneity*. However, when a reconstruction includes three or more tree species the scoring decreases to the point where it contributes to place the reconstruction in class D. Temporal clustering is present in most class C and D chronologies.

3.1.2. Sample replication

Reconstructions from Asia and Europe generally include more samples than reconstructions from North America (Table 4). Overall, mean replication is similar between Asia and Europe except for the sharp replication increase after c. 1850 in Europe at (Fig. 2). Noteworthy is also the decreasing sample replication towards the present in Asia as well as gradual post-1500 increase seen in many reconstructions from North America. The post-1850 replication increase in Europe biases the (20th century) calibration statistics – a feature absent in Asia and North America. Mean and maximum replication are highest in Europe and lowest in North America. The 11th/20th century ratio of the mean replication is highest, and with the largest spread, in Asia, and basically identical in Europe and North America (Fig. 5).

The reconstruction ranking highest in the category *Sample Replication* is the Northeastern Tibetan Plateau including 837 measurement series (Yang et al., 2014), followed by Central Europe (3124 series; Büntgen et al., 2011) and Colorado River (390 series; MacDonald et al., 2008). Reconstructions scoring well in *Sample Replication* are disproportionately often from Asia and Europe, whereas the majority of low scoring ones are from North America. The latter is even more apparent when considering the minimum replication: except two, all reconstructions including periods during which replication falls below 10 samples are from North America (Table 4).

3.1.3. Growth coherence

Mean Rbar values are highest in North America (0.42) and lowest in Europe (0.25), with values in Asia (0.38) closer to those of North America (Fig. 3; Fig. 6). The low Rbar values in Europe likely result from the inclusion of tree-ring material that is less homogeneous over time, including material derived from historical construction timber harvested over a wide region in different growth environment conditions. Another possible explanation for the low Rbar values in Europe is a lower proportion of the tree-ring material that is derived from arid or semi-arid environments.

Reconstructions scoring well in the category *Sample Replication* perform in some cases less well in the category *Growth Coherence* and vice versa. This is presumably related to data from sites, with various growth conditions, being included in many of the

Table 2

Abbreviations of tree species included in this study (see Table 1), used in the International Tree-Ring Data Bank (ITRDB; Grissino-Mayer and Fritts, 1997), following Grissino-Mayer (1993) with later updates. No refers to number of chronologies derived from the tree species.

Latin name	Common name	Family	Genera	ITRDB code	No
<i>Austrocedrus chilensis</i> (D.Don) Pic.Serm. & Bizzarri	Chilean cedar	Cupressaceae	<i>Austrocedrus</i>	AUCH	1
<i>Carya ovata</i> (Mill.) K.Koch	Shagbark hickory	Juglandaceae	<i>Carya</i>	CYOV	1
<i>Cedrus atlantica</i> Endl.	Atlas cedar	Pinaceae	<i>Cordia</i>	COAL	1
<i>Juniperus occidentalis</i> Hook	Western juniper	Cupressaceae	<i>Juniperus</i>	JUOC	3
<i>Juniperus osteosperma</i> (Torr.) Little	Utah juniper	Cupressaceae	<i>Juniperus</i>	JUOS	1
<i>Juniperus przewalskii</i> Kom.	Qilianshan juniper	Cupressaceae	<i>Juniperus</i>	JUPR	5
<i>Juniperus semiglobosa</i> Regel	Himalayan pencil juniper	Cupressaceae	<i>Juniperus</i>	JUSM	1
<i>Juniperus virginiana</i> L.	Eastern redcedar	Cupressaceae	<i>Juniperus</i>	JUVI	1
<i>Larix lyallii</i> Parl.	Alpine larch	Pinaceae	<i>Larix</i>	LALY	1
<i>Liriodendron tulipifera</i> L.	Tulip tree	Magnoliaceae	<i>Liriodendron</i>	LITU	1
<i>Magnolia accuminata</i> (L.) L.	Cucumbertree	Magnoliaceae	<i>Magnolia</i>	MAAC	1
<i>Picea mariana</i> (Mill.) Britton, Sterns & Poggenb.	Black spruce	Pinaceae	<i>Picea</i>	PCMA	1
<i>Picea rubens</i> Sarg.	Red spruce	Pinaceae	<i>Picea</i>	PCRU	1
<i>Pinus aristata</i> Engelm.	Rocky Mountain bristlecone pine	Pinaceae	<i>Pinus</i>	PIAR	2
<i>Pinus edulis</i> Engelm.	Colorado pinyon	Pinaceae	<i>Pinus</i>	PIED	3
<i>Pinus flexilis</i> E.James	Limber pine	Pinaceae	<i>Pinus</i>	PIFL	3
<i>Pinus heldreichii</i> Christ	Heldreich's pine	Pinaceae	<i>Pinus</i>	PIHE	1
<i>Pinus jeffreyi</i> A.Murray bis	Jeffrey pine	Pinaceae	<i>Pinus</i>	PIJE	2
<i>Pinus longaeva</i> D.K.Bailey	Intermountain bristlecone pine	Pinaceae	<i>Pinus</i>	PILO	3
<i>Pinus ponderosa</i> Douglas ex C.Lawson	Ponderosa pine	Pinaceae	<i>Pinus</i>	PIPO	6
<i>Pinus sibirica</i> (Ledeb.) Turcz.	Siberian stone pine	Pinaceae	<i>Pinus</i>	PISI	2
<i>Pinus strobiformis</i> Engelm.	Southwestern white pine	Pinaceae	<i>Pinus</i>	PISF	1
<i>Pinus sylvestris</i> L.	Scots pine	Pinaceae	<i>Pinus</i>	PISY	1
<i>Pseudotsuga menziesii</i> (Mirb.) Franco	Douglas fir	Pinaceae	<i>Pseudotsuga</i>	PSME	14
<i>Pinus monophylla</i> Torr. & Frém.	Singleleaf pinyon	Pinaceae	<i>Pinus</i>	PIMO	3
<i>Quercus alba</i> L.	White oak	Fagaceae	<i>Quercus</i>	QUAL	1
<i>Quercus douglasii</i> Hook. & Arn.	Blue oak	Fagaceae	<i>Quercus</i>	QUDG	1
<i>Quercus petraea</i> (Matt.) Liebl.	Sessile oak	Fagaceae	<i>Quercus</i>	QUPE	2
<i>Quercus prinus</i> L.	Chestnut oak	Fagaceae	<i>Quercus</i>	QUPR	1
<i>Quercus robur</i> L.	English oak	Fagaceae	<i>Quercus</i>	QURO	2
<i>Quercus sp.</i>	Oak	Fagaceae	<i>Quercus</i>	QUSP	2
<i>Sabina przewalskii</i> (Kom.) W.C.Cheng & L.K.Fu	Qilian juniper	Cupressaceae	<i>Sabina</i>	SBPI	2
<i>Tsuga canadensis</i> (L.) Carrière	Eastern hemlock	Pinaceae	<i>Tsuga</i>	TSCA	1
<i>Thuja occidentalis</i> L.	Northern white cedar	Cupressaceae	<i>Thuja</i>	THOC	1
<i>Taxodium distichum</i> (L.) Rich.	Baldcypress	Cupressaceae	<i>Taxodium</i>	TADI	5
<i>Taxodium mucronatum</i> Ten.	Montezuma bald cypress	Cupressaceae	<i>Taxus</i>	TACU	1

reconstruction with high replication resulting a weaker common signal. All reconstructions with the highest *Growth Coherence* (class A) come from North America. There is no consistent geographical pattern associated with those reconstructions with the lowest *Growth Coherence* (class D). Three reconstructions have negative *Rbar* values at some point during the past millennium (1000–2000 CE). Interestingly, these negative *Rbar* values do not necessarily appear in the, generally most weakly replicated, early part of the chronology.³

3.1.4. Chronology development

Whereas reconstructions from Europe are overrepresented among those with the highest *Chronology Development* scores (class A) several reconstructions from China ($n = 4$) and North America ($n = 7$) appear in class D (Table 6). The low *Chronology Development* scores are related to a large age range and a steep age trend in combination with individual detrending instead of RCS detrending (Fig. 3). An uneven age distribution also introduces a climate signal age effect bias (e.g., Linderholm and Linderholm, 2004; Rossi et al., 2008; Rozas et al., 2009; Čermák et al., 2019). Asian chronologies have the largest age range and age trend (Fig. 4) – as well as the

largest spread in both parameters – whereas European chronologies have the smallest age range and age trend (Fig. 7). The smaller observed average age trend in Europe, compared to Asia and North America, is related to the relative absence of long-lived tree species in Europe as well as due to the long history in Europe of intensive land use. The European chronologies have a flat age trend until the late nineteenth century in Europe, whereas in Asia the increase is visible already by c. 1300, and by c. 1700 in North America (Fig. 3). In addition, the spread in the age trend between chronologies from North America increases after c. 1600. All three continents have a strong age trend increase during the twentieth century. It is more common for chronologies from Europe to retain centennial to multi-centennial variability than for chronologies from Asia or North America as RCS has been applied to composite datasets.

3.1.5. Climate signal

All 12 reconstructions in the highest *Climate Signal* class A are from North America (Table 7). These reconstructions calibrate exceptionally well (mean 0.79 ± 0.07) against relatively long instrumental data (mean 96 ± 13 years) and in most cases the calibration/verification difference is a very small one (mean r. 0.08 ± 0.05) (Fig. 8). A very high correlation coefficient can compensate for a shorter calibration period and a larger calibration/verification difference. The reconstruction with the highest correlation to instrumental data (r. 0.90), the Bear River streamflow reconstruction (DeRose et al., 2015), has a calibration period of only 68 years and the calibration/verification difference is as large as r. 0.18, but is still placed in class A. There is an obvious overrepresentation of humid sites among those reconstructions with

³ The East Anglia precipitation reconstruction (Cooper et al., 2013) has a minimum *Rbar* value of -0.24 centered in the 1190s, the Jemez Mountain precipitation reconstruction (Touchan et al., 2011) has a minimum *Rbar* value of -0.22 centered in the 1430s, and the Central European precipitation reconstruction (Büntgen et al., 2011) a minimum *Rbar* value of -0.13 centered in the first decade of the nineteenth century.

Table 3

Data Homogeneity scores. Chronology type “C” refers to reconstructions derived from a composite of material from living trees, remnant, historical and/or sub-fossil wood. Type “L” refers to reconstructions derived from only living trees. Temporal clustering (Yes) indicates reconstructions composed of data from distinct sites or species concentrated in discrete periods over the past 1000 years. Other abbreviations: AM = archeological material; HM = historical material; RM = remnant material; SF = subfossil material (MacDonald and Case, 2005). (For interpretation of the references to color in this table legend, the reader is referred to the Web version of this article.)

6. Homogeneity									
5. Remark									
4. Temporal clustering									
3. Species number									
2. Chronology type									
1. Source									
A'nyêmaqên, China	L, 1 site	L	1	No	Site at the lowest forest border on a south-facing slope				●
Bear River, USA	1 site	C	1	No	From south-facing slopes on one site				●
Hexi Corridor, China	L, 1 site	L	1	No	From open stands 3000–3520 m a.s.l.				●
Khorgo, Mongolia	1 site	C	1	No	Stunted trees growing on basaltic lava				●
Mount San Gorgonio	1 site	C	1	No	New measurements combined with old ones from the 1970s				●
Pamir-Alay Mountains, Tajikistan	L, 1 site	L	1	No	Sampled trees grow on a southern exposure 30–40° slope				●
Southern Sierra Nevada, USA	1 site	C	1	No	Only 3 radii in 1000 CE, increasing correlation back in time				●
Summitville, USA	1 site	C	1	No	Based on relatively few trees				●
Tavaputs Plateau, USA	L and RM, 2 sites	C	1	No	Merged into the Harmon Canyon chronology				●
Uurgat, Mongolia	1 site	C	1	No	Stunted trees growing on basaltic lava				●
White Mountains, USA	1 site	C	1	No	Very old trees from small area				●
Albamarle Sound, USA	2 sites	C	1	No	Combination of two chronologies				●
Atlas Mountains, Morocco	L, several sites	L	1	Yes	Pre-1200 data dominated by one site				●
Barranca de Amealco, Mexico	1 site	C	1	Yes	Jump from lower to higher TRW level in 16 th century				●
Central Chile	2 sites	C	1	Yes	Data from two rather nearby sites				●
Choctawhatchee River, USA (EW)	SF, 2 sites	C	1	No	EW data from two river systems in Florida and Georgia				●
Choctawhatchee River, USA (LW)	SF, 2 sites	C	1	No	EW data from two river systems in Florida and Georgia				●
Delingha, China	L, 7 sites	L	1	No	Maximum distance between sites is 137 km				●
El Malpais, USA	2 sites	C	2	No	Temporal coverage of the two species unclear				●
El Malpais, USA (EW)	2 sites	C	2	No	Include data from Grissino-Mayer (1995) plus new living material				●
El Malpais, USA (LW)	2 sites	C	2	No	Include data from Grissino-Mayer (1995) plus new living material				●
Flowerpot, Canada	1 site	C	1	No	Severely changing microsite conditions				●
Heihe River Basin, China	3 sites	L	1	No	Merged Hegershoff and negative exponential sub-chronologies				●
Mount Smolikas, Greece	8 sites	C	1	No	Small micro-site differences exist				●
Whirlpool point, Canada	1 site	C	2	No	Also used in MacDonald and Case (2005) for reconstructing PDO				●
Central Europe	HM, multiple sites	C	1	No	Data from numerous sites across Central Europe				●
Dulan, China	HM, several sites	C	1	Yes	Historical material from lower elevations				●
East Anglia, UK	HM, multiple sites	C	2	Yes	Multiple sites from homogeneous region				●
Georgia, USA	3 sites	C	1	Yes	Based on only one site before 1206				●
Little Snake River, USA	5 sites over a large area	C	2	Yes	Same tree-ring data used for three reconstructions				●
Mesa Verde, USA (EW)	5 sites: L, RM and AM	C	1	Yes	Archeological wood only prior to 1250 CE				●
Mesa Verde, USA (LW)	5 sites: L, RM and AM	C	1	Yes	Archeological wood only prior to 1250 CE				●
Northeastern Tibetan Plateau, China	17 sites L and 5 sites AM	C	1	Yes	Trees growing from 3200–4200 m a.s.l.				●
Qilian Mountains, China	Living trees, 3 sites	L	1	Yes	One site not covering the whole 11 th century				●
Southern Colorado Plateau, USA	RM, multiple sites	C	2	Yes	Sites treated separately, and combined to one reconstruction				●
Southern Finland	L and RM, 3 sites	C	1	Yes	From 61°–62°N, 29°–28°E				●
Southerncentral England, UK	HM, multiple sites	C	2	Yes	Multiple sites from larger region, 15 living tree sites				●
White River, USA	5 sites from large area	C	2	Yes	Same tree-ring data used for three reconstructions				●
Yampa River, USA	5 sites from large area	C	2	Yes	Same tree-ring data used for three reconstructions				●
Colorado River, USA	11 sites	C	5	No	Predictor pooled from a very wide area				●
Jemez Mountains, USA	5 sites	C	3	Yes	Only one site extends back to 1000 CE				●
Lee Ferry, USA	11 sites	C	2	Yes	Widely dispersed sites in Colorado River watershed region				●
Potomac River, USA	27 sites	C	9	Yes	More sites and species than in any other reconstruction				●
Sacramento River, USA	7 sites	C	3	No	Predictor pooled from a very wide area				●
Upper Arkansas River Basin, USA	8 sites	C	3	Yes	Eight sites located long from each other of three species				●
Upper Klamath River Basin, USA	17 sites	C	4	Yes	Predictor pooled from a very wide area				●

● Class A ● Class B ● Class C ● Class D

Table 4

Sample Replication scores. The number of measurement series included in the reconstructions. 11th/20th is the ratio of the mean replication during the 11th century relative to the mean replication during the 20th century. (For interpretation of the references to color in this table legend, the reader is referred to the Web version of this article.)

5. Replication					
4. 11 th /20 th [%]					
3. Minimum					
2. Maximum					
1. Mean					
Northeastern Tibetan Plateau, China	628	810	266	69	●
Central Europe	337	502	58	76	●
Khorgo, Mongolia	64	82	42	127	●
Colorado River, USA	284	362	12	62	●
Sacramento River, USA	175	253	42	43	●
Heihe River Basin, China	116	160	52	114	●
Delingha, China	236	275	101	60	●
Southern Finland	122	265	26	40	●
Dulan, China	154	216	42	35	●
Southerncentral England, UK	198	349	51	22	●
East Anglia, UK	89	306	11	31	●
Hexi Corridor, China	124	203	13	17	●
El Malpais, USA	81	123	18	49	●
Flowerpot, Canada	50	111	15	57	●
Urgat, Mongolia	31	40	24	93	●
Mount Smolikas, Greece	195	363	39	13	●
White Mountains, USA	45	56	15	65	●
A'nyêmaqên, China	58	83	21	41	●
Tavaputs Plateau, USA	24	29	18	92	●
Choctawhatchee River, USA (EW)	36	51	8	3	●
Lee Ferry, USA	194	355	29	9	●
Southern Colorado Plateau, USA	194	355	29	9	●
Barranca de Amealco, Mexico	23	36	12	63	●
Summitville, USA	12	14	9	115	●
Albemarle Sound, USA	39	58	13	34	●
Whirlpool point, Canada	50	94	16	23	●
Qilian Mountains, China	42	68	13	28	●
Georgia, USA	58	87	10	2	●
Bear River, USA	20	45	9	37	●
Choctawhatchee River, USA (LW)	33	49	8	3	●
Mount San Geronio	17	24	6	27	●
El Malpais, USA (EW)	25	66	8	23	●
El Malpais, USA (LW)	23	50	8	26	●
Atlas Mountains, Morocco	134	294	3	4	●
Potomac River, USA	104	309	9	4	●
Central Chile	17	24	6	27	●
Pamir-Alay Mountains, Tajikistan	32	63	4	9	●
Little Snake River, USA	98	104	5	4	●
White River, USA	98	104	5	4	●
Yampa River, USA	98	104	5	4	●
Upper Arkansas River Basin, USA	13	18	3	22	●
Southern Sierra Nevada, USA	14	33	3	13	●
Mesa Verde, USA (EW)	23	52	5	8	●
Mesa Verde, USA (LW)	23	52	5	8	●
Jemez Mountains, USA	59	208	3	2	●
Upper Klamath River Basin, USA	14	32	6	8	●

● Class A

● Class B

● Class C

● Class D

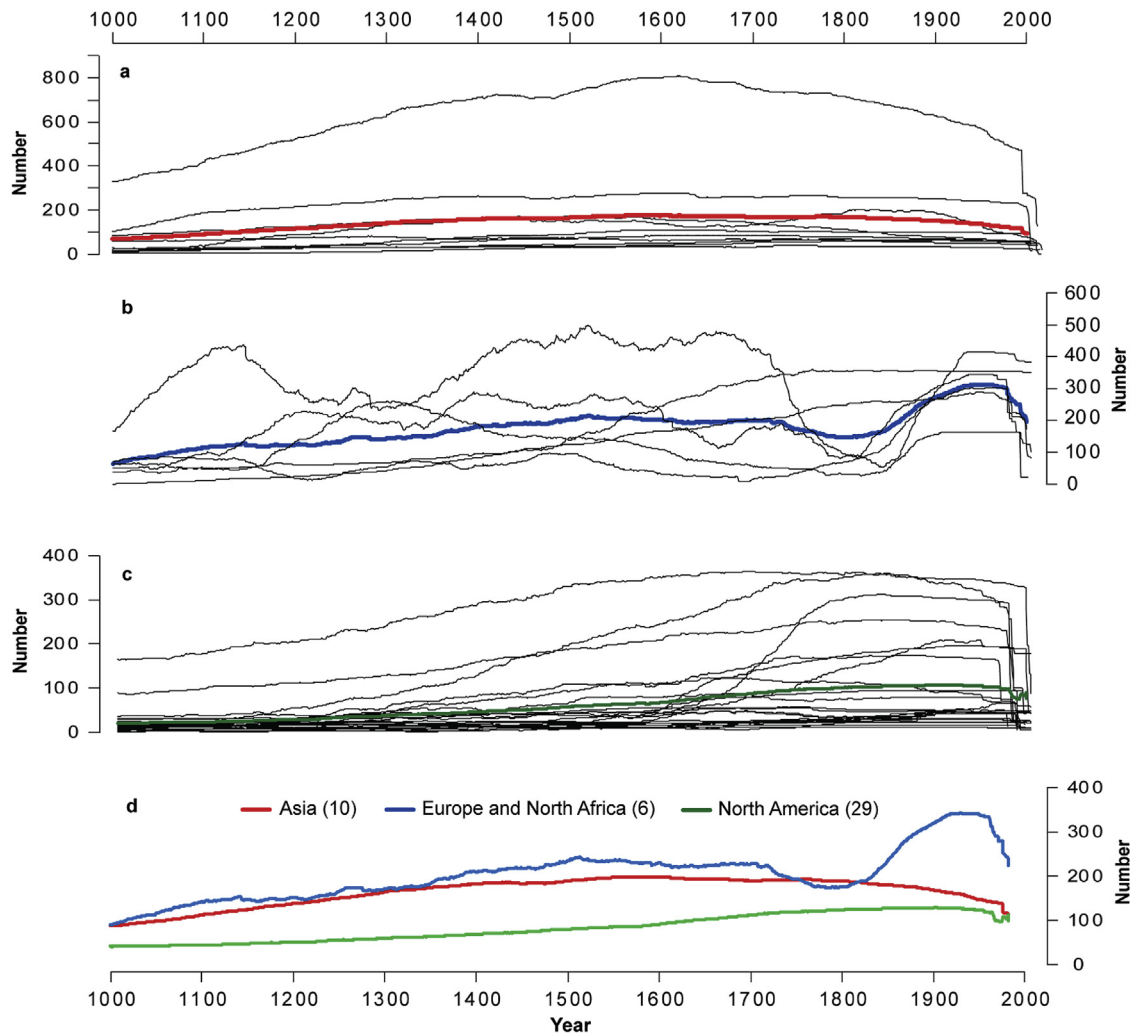


Fig. 2. Tree-ring chronology replication curves. Thin black curves show the changing number of tree-ring width measurement series within the hydroclimate reconstructions from Asia (a), Europe and North Africa (b), and North America (c). The colored curves represent the arithmetic means calculated over the common period covered by all reconstructions in each of the three regions. (d) Comparison of the mean curves for Europe/North Africa, Asia, and North America.

the lowest *Climate Signal* scores (class D). The eleven reconstructions of the lowest *Climate Signal* class D are characterized by comparatively low correlation values to their instrumental targets ($r. 0.63 \pm 0.09$), rather large calibration/verification differences ($r. 0.14 \pm 0.08$), but highly variable calibration period lengths ranging from 34 to 115 years. The calibration period of all *Climate Signal* class D reconstructions has been truncated due to a “divergence” problem. In Asia, the short calibration periods stand out, but the correlation values are similar to those of North America. The reconstructions from Europe are typically calibrated over periods of similar length as those for North America but correlation values are lower (Fig. 8c). It can be noted that the majority of the evaluated hydroclimate tree-ring records show a weak – mostly insignificant – negative correlation to local annual mean temperature over the twentieth century, with a mean of -0.12 and a range from -0.01 and -0.25 between the first and the third quartiles.

3.2. Overall tree-ring hydroclimate reconstruction ranking

The results from our assessment of *Data Homogeneity*, *Sample*

Replication, *Growth Coherence*, *Chronology Development*, and *Climate Signal* of 46 millennium-long tree-ring based hydroclimate reconstructions are presented in Tables 3–7. Clear differences between reconstructions become apparent in the overall tree-ring chronology ranking shown in Table 8. Two reconstructions, Khorgo and Uurgat (Hessl et al., 2018), score high (class A or class B) in all five categories. Nine reconstructions score high (class A or class B) in four of out five categories. Eleven reconstructions score less well (class C and class D) in at least four out of five categories.

Some reconstructions score high in some parameters and low in some others. The most notable example is the Central Europe precipitation reconstruction (Büntgen et al., 2011). It ranks #1 in *Chronology Development* and #2 in *Sample Replication*, but #45 in *Growth Coherence* and #44 in *Climate Signal*. Another reconstruction, Southern Sierra Nevada (Graumlich, 1993), scores the highest (class A) in all categories except in *Sample Replication* where it scores the lowest (class D). Conversely, the Colorado River reconstruction (MacDonald et al., 2008) scores low (class D) in all categories except in *Sample Replication* where it scores high (class A).

No geographical differences are apparent in the overall tree-ring

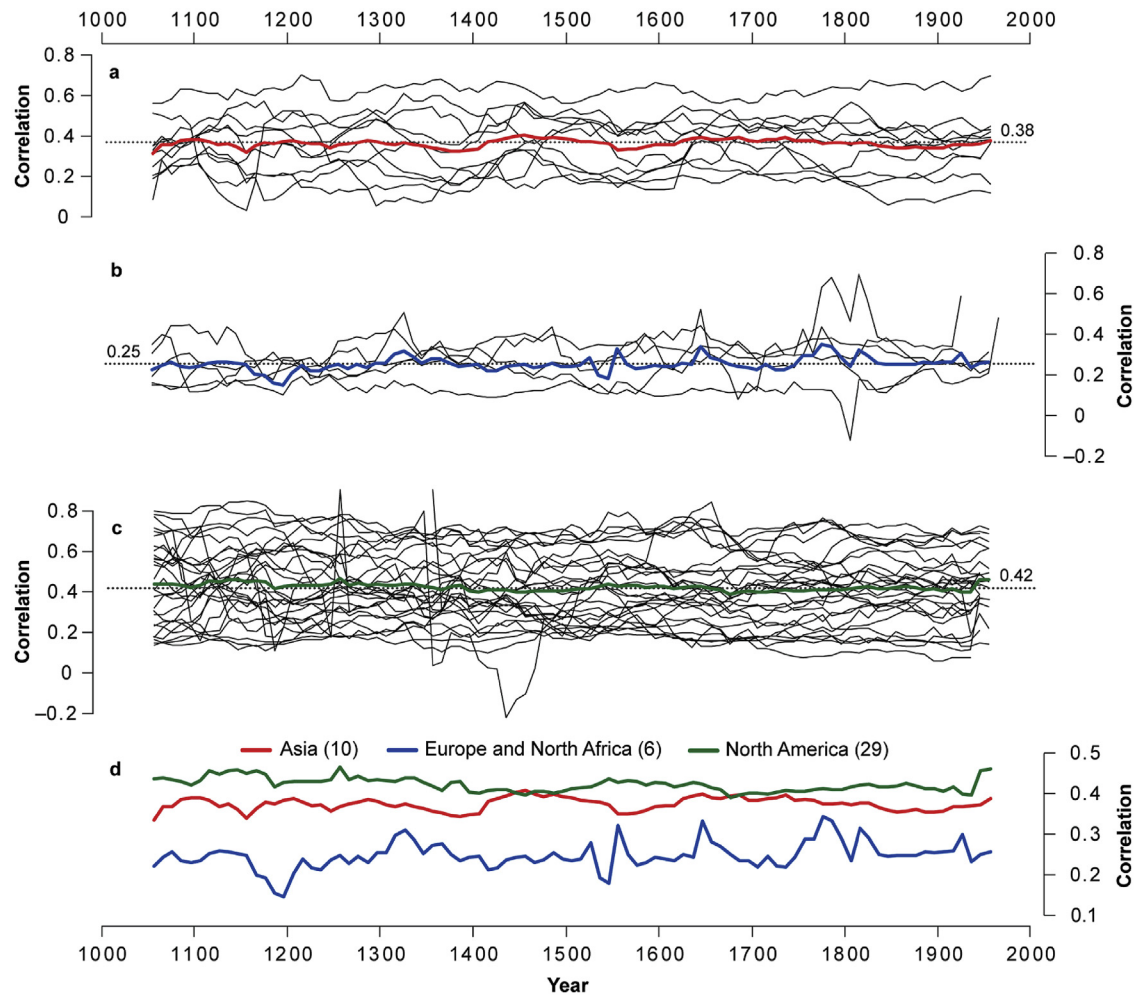


Fig. 3. Tree-ring chronology inter-series correlations. Thin black curves show the correlation coefficients among the tree-ring width measurement series used in the local hydroclimate reconstructions from Asia (a), Europe and North Africa (b), and North America (c). Correlations are calculated over 100-year periods shifted in 10-year steps throughout the past millennium (from 1000 CE to the end of the chronology). The earliest value is centered on 1050 CE, the most recent value on 1950 CE. Colored curves represent the arithmetic means calculated for each of the three regions, and the dashed black lines indicate the mean values over the past millennium. (d) Comparison of the mean inter-series correlation curves for Europe/North Africa, Asia, and North America.

hydroclimate reconstruction ranking. However, with only a few exceptions – e.g., two reconstructions from humid United Kingdom – reconstructions from arid and semi-arid environments dominate those in class A. Reconstructions from humid environments are on the other hand overrepresented in class D, although several reconstructions from arid and semi-arid environments are also found there. We also find that recently developed reconstructions are not necessarily better than older ones, except for the ability to preserve low-frequency information. Three of the highest-ranking reconstructions – El Malpais (Grissino-Mayer, 1995), Southern Sierra Nevada (Graumlich, 1993) and White Mountains (Hughes and Graumlich, 1996) – were actually among the earliest developed millennium-long hydroclimate reconstructions.

4. Discussion

4.1. Implications of the ranking of hydroclimate reconstructions

This article attempts to provide an objective evaluation of the

strength and weakness of millennium-long tree-ring based hydroclimate reconstructions. Our ranking offers guidance for users of these reconstructions inside and outside the dendroclimatological community. It emphasizes the complexity of a comprehensive assessment in which the correlation with instrumental data – arguably the most intuitive quality criterion – is only one out of many aspects. In practice, different research questions will pose different selection criteria so that the ranking presented here will be not equally applicable to all dendroclimatological studies. For example, if the objective is to infer the influence of drought stress on long-term agricultural productivity, it is desirable to select the best, regionally representative, reconstruction. Furthermore, if the focus is on the effect of climatic extreme events, a lack of low-frequency information may be less of a problem. On the other hand, a wide spatial coverage, even sample replication over time, and preserved low-frequency information, are desirable if the goal is to investigate where warm–wet and warm–dry associations tend to occur or to understand the synoptic climate situations and feedback mechanisms responsible for such patterns. The design of our

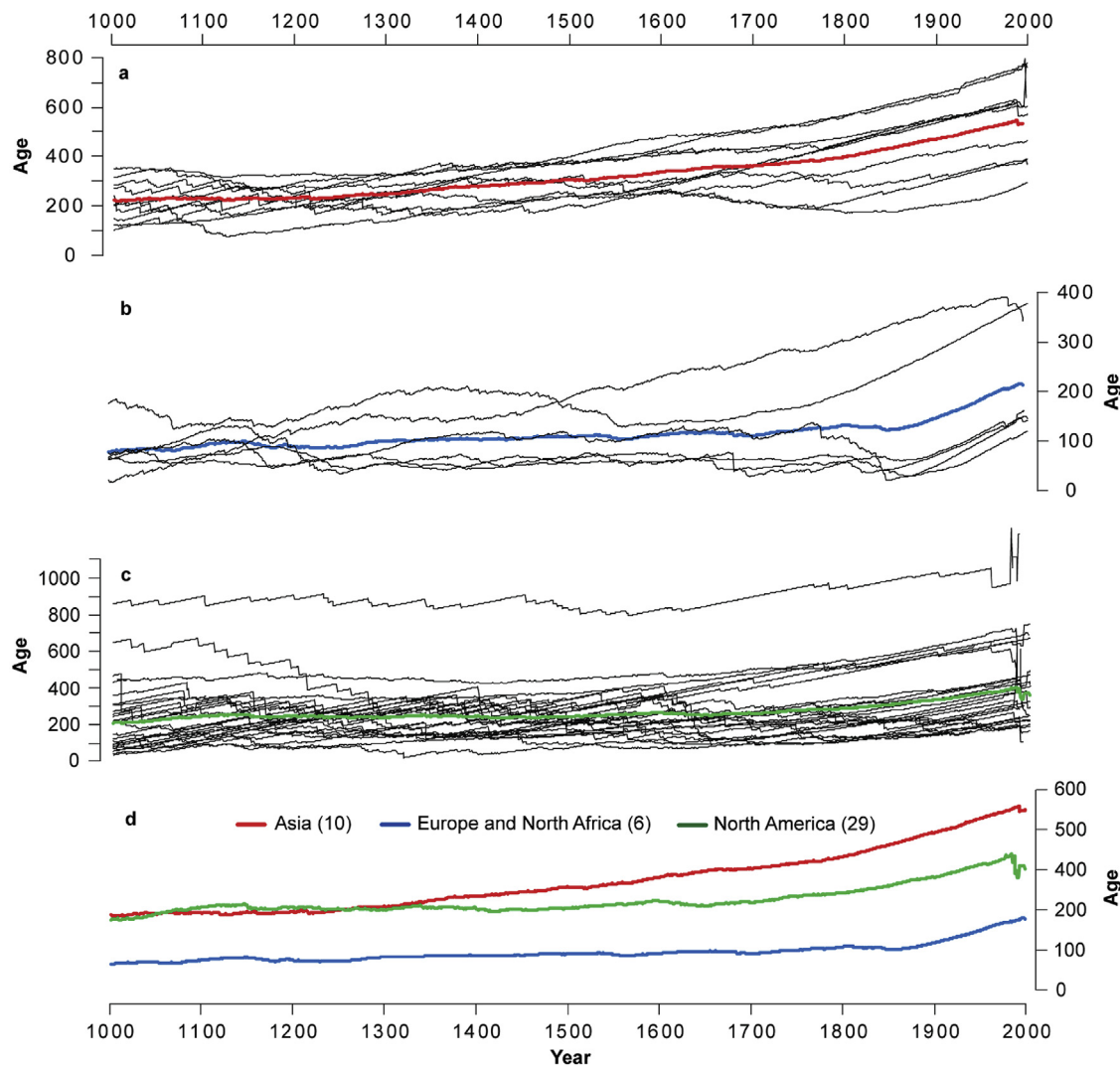


Fig. 4. Tree-ring chronology age curves. Thin black curves show the mean tree age of the tree-ring width data used in the local hydroclimate reconstructions from Asia (a), Europe and North Africa (b), and North America (c). Colored curves are the arithmetic means calculated over the common period covered by all reconstructions in each of the three regions. (d) Comparison of mean replication curves for Europe/North Africa, Asia, and North America.

criteria includes variability at timescales from inter-annual to multi-centennial, with a specific accentuation on the lower frequencies that cannot be controlled in the period of instrumental overlap. An issue to consider is that poor replication during the first centuries, compared to the (20th century) calibration period, makes the quantification of the severity of medieval megadroughts or enhanced monsoon precipitation in comparison to recent “extremes” uncertain. In this context, it can also be noted that several reconstructions, published as millennium-long, were excluded from this assessment as they either stopped just short of 1000 CE or did not have the sufficient replication (of at least three samples) all the way back to 1000 CE (e.g., Büntgen et al., 2010a,b; Stambaugh et al., 2011). The threshold of at least three measurement series is set rather low. Generally speaking, at least 10 ring width measurement series from different trees ought to be included in a reliable reconstruction, though the precise number depends on the inter-series correlation (R_{bar}) and the climate signal strength inherent to the particular data.

Hydroclimate is a complex climatological metric as it includes precipitation, soil moisture and temperature-driven evapotranspiration. It also possesses a higher spatial heterogeneity than temperature and a multi-faceted spectral character. The much shorter spatial co-variance of precipitation and all other metrics of hydroclimate compared to temperature makes it less feasible than for temperature to only include the highest-ranking hydroclimate reconstructions in further assessments or large-scale reconstructions. In the interpretation of the low-frequency hydroclimate variability it is important to consider to what extent a reconstruction actually preserves information on longer than multi-decadal time-scales. We here identified a problematic feature with the tree-ring based hydroclimate reconstructions, as opposed to most state-of-the-art tree-ring based temperature reconstructions, in the low proportion of reconstructions produced through RCS. The general application of individual-series detrending methods to produce most of the hydroclimate reconstructions risk removal of centennial-scale variability. Including “noisy” reconstructions, with only a few

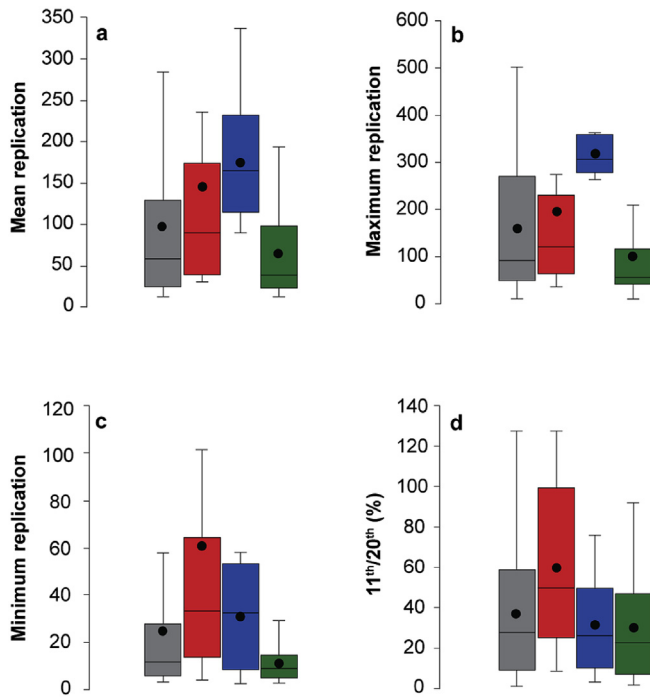


Fig. 5. Box plot figures showing the distribution of *Sample Replication* scores for all 46 reconstructions (grey), Asia (red), Europe and North Africa (blue), and North America (green) with a box drawn between the first and third quartiles, a line across the box shows the median, the black dot shows the mean, and minimum and maximum values indicated by whiskers. (a) Mean replication. (b) Maximum replication. (c) Minimum replication. (d) The ratio of the mean replication during the 11th century relative to the mean replication during the 20th century.

measurement series back in time, does not necessarily improve any network analysis. It is rather recommended to evaluate each individual chronology and include only those reconstructions that can be expected to include relevant information. Thus, data selection based on only the calibration statistics is not recommended.

Evaluating the robustness of the tree-ring based reconstructions based on other types of hydroclimate proxy records is unfortunately difficult for several reasons (and cannot thus be turned into an evaluation criteria). Tree-ring records are by far the most abundant natural climate archive with a temporal resolution and age control that allows for calibration and validation against instrumental observations. For many of the evaluated tree-ring chronologies, there exists no other comparable calibrated proxy record in the region. Investigating the agreement of the low-frequency signal in the hydroclimate reconstructions with that of lower resolution records is not as straightforward option as it may appear. Recent studies (e.g., Schneider et al., 2019) show that a robust quality estimation requires a very dense proxy network, composed of many various archives, rather than a single neighboring proxy record.

The frequently short and unevenly distributed meteorological station data in Asia (normally starting after 1950) pose severe constraints on the calibration and verification statistics for this portion of the hydroclimate network. Several reconstructions from Asia – most notably the one from the Northeastern Tibetan Plateau (Yang et al., 2014), reaching a correlation to instrumental precipitation data of $r = 0.84$, would rank high in the category *Climate Signal* along with the records from North America, if a longer (reliable)

instrumental calibration period was available. Allowing for a 100-year long calibration period would potentially score the Northeastern Tibetan Plateau (Yang et al., 2014), Heihe River Basin (Yang et al., 2012), Khorgo and Uurgat (Hessl et al., 2018) in *Climate Signal* class A. Likewise, it could improve the ranking of A'nyemaqen (Gou et al., 2010), Delingha (Shao et al., 2005), Hexi Corridor (Yang et al., 2019), and Qilian Mountains (Zhang et al., 2011).

4.2. Comparison with the temperature reconstruction ranking

Unlike the tree-ring based temperature reconstructions (Esper et al., 2016), the hydroclimate reconstructions can include more (up to nine) species (Table 2). The largest difference between the ranking of the hydroclimate and temperature reconstructions is found for *Sample Replication*. A similar replication for the chronologies between continents is found for temperature reconstructions, compared to a much higher replication for Asia and Europe and a lower replication for North America for hydroclimate reconstructions. The relative *Growth Coherence* between continents are, on the other hand, similar for the hydroclimate and temperature reconstructions, with the lowest values for Europe and comparable ones for Asia and North America. The highest *Chronology Development* scores, with the smallest spread, are found in Europe for both hydroclimate and temperature reconstructions. A larger *Chronology Development* spread is evident for hydroclimate reconstructions in Asia and for temperature reconstructions in North America. *Climate Signal* scores are similar for each continent in both the hydroclimate and temperature reconstructions, with Europe having overall the highest scores (Fig. 9).

Severe climatic conditions for tree growth at the species' distribution limit (Fritts, 1976) resulted in the highest *Growth Coherence* scores for both tree-ring based hydroclimate and temperature reconstructions. The twelve *Growth Coherence* best-scoring hydroclimate reconstructions are from arid or semi-arid environments in the southwestern United States (see e.g., St George, 2014; St George and Ault, 2014), whereas the three best-scoring temperature reconstructions are all from northern Siberia: Indigirka (Sidorova et al., 2006), Yamal (Briffa et al., 2013), and Taimyr (Briffa et al., 2008). The trees included in these reconstructions, growing in a shallow active layer in the continuous permafrost zone, likely experience a shorter growing season than any of the other temperature reconstructions included in Esper et al. (2016).

The four highest-ranking reconstructions in the category *Chronology Development*, both for hydroclimate and temperature, are from Europe. For hydroclimate, it is Central Europe (Büntgen et al., 2011), East Anglia (Cooper et al., 2013), Southern Finland (Helama et al., 2009), and Southcentral England (Wilson et al., 2013), whereas for temperature it is Northern Scandinavia (Esper et al., 2012), Finland (Helama et al., 2010), tree-ring width version of Torneträsk (Melvin et al., 2013), and Lötschental (Büntgen et al., 2006). High scores in *Chronology Development* typically result from a combination of a small age range and minor linear trends in mean age curve over the past millennium, in combination with the application of RCS detrending, to emphasize centennial to multi-centennial climate variability.

Overall, the average correlation between the tree-ring reconstructions and the instrumental data is higher for hydroclimate reconstructions (mean $r = 0.69 \pm 0.11$) than for temperature reconstructions ($r = 0.59 \pm 0.15$), which perhaps appears surprising given the spatially homogeneous nature of hydroclimate. The region with the generally highest relationship between tree growth and hydroclimate is found in the southwestern United States (see, e.g., St George, 2014; St George and Ault, 2014) whereas the highest

Table 5

Growth Coherence scores. Mean, maximum, and minimum correlations among the series included in the reconstructions. 11th/20th is the ratio of the correlation during the 11th century relative to the 20th century correlation. (For interpretation of the references to color in this table legend, the reader is referred to the Web version of this article.)

5. Growth coherence					
4. 11 th /20 th [%]					
3. Minimum					
2. Maximum					
1. Mean					
El Malpais, USA (EW)	0.72	0.83	0.63	112%	●
Upper Arkansas River Basin, USA	0.50	0.78	0.30	150%	●
Upper Klamath River Basin, USA	0.66	0.78	0.52	113%	●
Whirlpool point, Canada	0.57	0.68	0.47	123%	●
El Malpais, USA	0.67	0.75	0.57	104%	●
Southern Sierra Nevada, USA	0.36	0.77	0.15	150%	●
Tavaputs Plateau, USA	0.64	0.73	0.50	102%	●
Choctawhatchee River, USA (EW)	0.40	0.58	0.27	150%	●
Summitville, USA	0.50	0.63	0.36	122%	●
White Mountains, USA	0.51	0.59	0.39	121%	●
Bear River, USA	0.62	0.84	0.42	93%	●
Mesa Verde, USA (EW)	0.69	0.85	0.54	78%	●
Khorgo, Mongolia	0.58	0.66	0.52	83%	●
Jemez Mountains, USA	0.44	0.80	-0.22	132%	●
Potomac River, USA	0.26	0.56	0.06	150%	●
A'nyêmaqên, China	0.43	0.54	0.35	92%	●
Dulan, China	0.40	0.46	0.31	100%	●
Delingha, China	0.44	0.54	0.33	82%	●
Uurgat, Mongolia	0.45	0.57	0.32	78%	●
El Malpais, USA (LW)	0.43	0.59	0.26	80%	●
Heihe River Basin, China	0.23	0.36	0.13	139%	●
Northeastern Tibetan Plateau, China	0.27	0.35	0.20	115%	●
Mount San Gorgonio, USA	0.36	0.73	0.19	72%	●
Atlas Mountains, Morocco	0.29	0.40	0.11	113%	●
East Anglia, UK	0.20	0.76	-0.24	124%	●
Choctawhatchee River, USA (LW)	0.29	0.47	0.22	89%	●
Mesa Verde, USA (LW)	0.44	0.60	0.29	59%	●
Qilian Mountains, China	0.32	0.45	0.21	72%	●
Southerncentral England, UK	0.15	0.29	0.08	133%	●
Georgia, USA	0.33	0.39	0.20	74%	●
Lee Ferry, USA	0.33	0.39	0.20	74%	●
Central Chile	0.23	0.34	0.15	91%	●
Southern Colorado Plateau, USA	0.32	0.28	0.22	77%	●
Mount Smolikas, Greece	0.28	0.43	0.17	71%	●
Barranca de Amealco, Mexico	0.22	0.48	0.11	76%	●
Albemarle Sound, USA	0.21	0.36	0.14	85%	●
Little Snake River, USA	0.40	0.62	0.17	50%	●
White River, USA	0.40	0.62	0.17	50%	●
Yampa River, USA	0.40	0.62	0.17	50%	●
Hexi Corridor, China	0.36	0.57	0.15	51%	●
Flowerpot, Canada	0.24	0.49	0.10	58%	●
Sacramento River, USA	0.17	0.30	0.13	66%	●
Pamir-Alay Mountains, Tajikistan	0.28	0.54	0.11	42%	●
Southern Finland	0.33	0.69	0.15	30%	●
Colorado River, USA	0.18	0.37	0.11	44%	●
Central Europe	0.13	0.23	-0.13	72%	●



Class A



Class B



Class C



Class D

Table 6

Chronology Development scores. Detrending method 1 = RCS (and Signal Free), and 2 = individual detrending. Age range is the difference between highest and lowest point on the mean age curve over the past millennium. Age trend is the slope of a linear regression fit to the mean age curve over the past millennium (times 100). Maximum frequency indicates the wavelength of lowest frequency information retained in a reconstruction, with 1 = centennial to multi-centennial, and 2 = decadal to centennial. (For interpretation of the references to color in this table legend, the reader is referred to the Web version of this article.)

5. Chronology development					
4. Maximum frequency					
3. Age trend					
2. Age range [yrs.]					
1. Detrending method					
Central Europe	1	98	−0.04	1	●
East Anglia, UK	1	121	−0.68	1	●
Southern Finland	1	138	1.44	1	●
Southerncentral England, UK	1	109	2.13	1	●
Urgat, Mongolia	2	209	2.18	2	●
Upper Klamath River Basin, USA	2	279	2.06	2	●
Hexi Corridor, China	1	224	10.92	1	●
Whirlpool point, Canada	2	287	6.38	1	●
Southern Sierra Nevada, USA	2	281	3.66	2	●
Summitville, USA	2	431	6.60	1	●
Khorgo, Mongolia	2	348	3.86	2	●
Mount Smolikas, Greece	1	256	−9.07	2	●
El Malpais, USA (LW)	2	227	−6.15	2	●
Flowerpot, Canada	2	327	−5.67	2	●
Northeastern Tibetan Plateau, China	1	301	26.22	1	●
Potomac River, USA	2	388	5.97	2	●
White Mountains, USA	2	476	12.36	1	●
Mesa Verde, USA (LW)	2	250	−8.86	2	●
Bear River, USA	2	325	−7.83	2	●
Mesa Verde, USA (EW)	2	261	−9.07	2	●
El Malpais, USA (EW)	2	240	−9.55	2	●
Barranca de Amelco, Mexico	2	243	9.52	2	●
Atlas Mountains, Morocco	1	371	34.17	1	●
Sacramento River, USA	2	212	12.03	2	●
Tavaputs Plateau, USA	2	297	10.84	2	●
Choctawhatchee River, USA (EW)	2	217	13.12	2	●
Choctawhatchee River, USA (LW)	2	226	13.17	2	●
Albemarle Sound, USA	2	250	13.83	2	●
Jemez Mountains, USA	2	269	−15.42	2	●
Pamir-Alay Mountains, Tajikistan	2	422	28.71	1	●
Heihe River Basin, China	1	582	50.30	1	●
El Malpais, USA	2	308	19.48	2	●
Southern Colorado Plateau, USA	2	321	20.63	2	●
Lee Ferry, USA	2	322	20.63	2	●
Central Chile	1	462	35.48	2	●
Mount San Geronio, USA	2	463	35.48	1	●
Upper Arkansas River Basin, USA	2	585	40.51	1	●
Little Snake River, USA	2	372	29.09	2	●
White River, USA	2	372	29.09	2	●
Yampa River, USA	2	372	29.09	2	●
Georgia, USA	2	274	35.50	2	●
Qilian Mountains, China	2	376	33.47	2	●
Colorado River, USA	2	469	33.69	2	●
Dulan, China	2	465	42.36	2	●
A'nyemaqên, China	2	634	40.65	2	●
Delingha, China	2	678	62.75	2	●



Class A



Class B



Class C



Class D

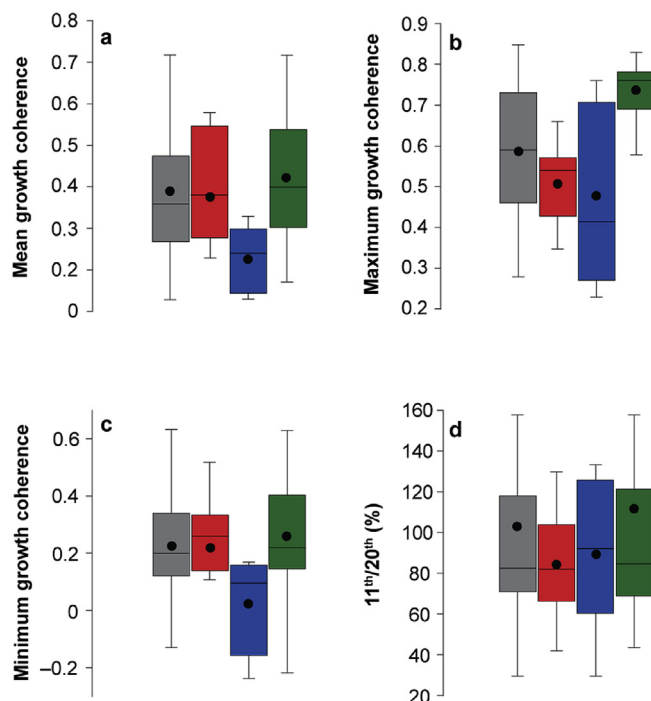


Fig. 6. Box plot figures showing the distribution of *Growth Coherence* scores for all 46 reconstructions (grey), Asia (red), Europe and North Africa (blue), and North America (green) with a box drawn between the first and third quartiles, a line across the box shows the median, the black dot shows the mean, and minimum and maximum values indicated by whiskers. (a) Mean Rbar. (b) Maximum Rbar. (c) Minimum Rbar. (d) The ratio of the mean Rbar during the 11th century relative to the mean Rbar during the 20th century.

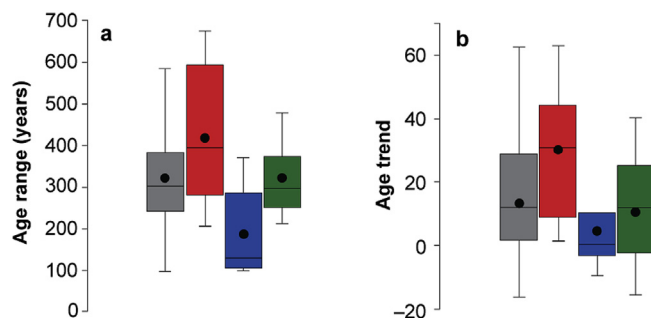


Fig. 7. Box plot figures showing the distribution of *Chronology Development* scores for all 46 reconstructions (grey), Asia (red), Europe and North Africa (blue), and North America (green) with a box drawn between the first and third quartiles, a line across the box shows the median, the black dot shows the mean, and minimum and maximum values indicated by whiskers. (a) Age range between the highest and lowest point on the mean age curve over the past millennium. (b) Age trend as a slope of a linear regression fit to the mean age curve over the past millennium (times 100).

relationship between tree growth and temperature is generally found in high latitude Eurasia and in the European Alps (Esper et al., 2016). The calibration period is generally shorter for the hydroclimate reconstructions (mean 79 ± 23 years) than for temperature reconstructions (mean 101 ± 43 years). This provides a larger challenge to skillfully calibrate especially the low-frequency component of hydroclimate variability. Typically, precipitation measurements are either shorter or contain more noise prior to the

twentieth century than temperature measurements (Pauling et al., 2006; Harris et al., 2014).

4.3. Expansion of the hydroclimate tree-ring reconstruction network

At present, millennium-long tree-ring based reconstructions with a well-verified hydroclimate signal are only available from few locations in the world (Fig. 1; Fig. 10). As tree-ring records are the only natural hydroclimate proxy with annual resolution and exact dating control, there is an urgent need to expand this network. From more mesic locations there is a general challenge to extend hydroclimate tree-ring records back in time, as they offer generally less favorable conditions for wood preservation. In China, subfossil woods in lake or river sediments are difficult to find (He et al., 2019), and old living trees and remnant woods can mainly be collected in the dry parts of the country (Liu et al., 2019). In some places, not least in Europe, tree-ring based reconstructions can be extended with wood from archeological sites and old buildings (Tegel et al., 2010).

An additional challenge is posed by the decrease in hydroclimate sensitivity of tree growth in cool and wet environments. One solution to this problem is to reconstruct soil moisture availability using tree-ring data from temperature-limited environments by considering the pivotal role of surface temperature in determining the land surface heat flux, evapotranspiration and consequently the water balance (Cook et al., 2015a,b; Seftigen et al., 2015a,b). However, such reconstructions need to be treated with caution – both Baek et al. (2017) and Ljungqvist et al. (2019) found that they may overestimate the influence of temperature variability on soil moisture. Moreover, temperature and precipitation contain different spectral characteristics, where the former contains larger low-frequency loadings than the latter (Bunde et al., 2013; Franke et al., 2013; Zhang et al., 2015), making it problematic to use temperature-sensitive tree-ring data for hydroclimate reconstructions.

Despite such constraints, it has been demonstrated that tree-ring chronologies with a strong hydroclimatic signal can be developed in cooler and wetter environments. Hydroclimate reconstructions have been developed in Scandinavia spanning the past three to five centuries (see e.g., Helama and Lindholm, 2003; Linderholm et al., 2004; Jönsson and Nilsson, 2009; Drobyshev et al., 2011; Seftigen et al., 2015a; 2015b). The potential to develop millennium-long reconstructions is evident from the Helama et al. (2009) May–June precipitation reconstruction from south-east Finland. In European Russia (52–57°N, 35–52°E), most tree-ring chronologies have been shown to correlate weakly but significantly with hydroclimate (Matskovsky, 2016; Matskovsky et al., 2017; Solomina et al., 2017), but all the available hydroclimate tree-ring reconstructions at present only reach back to the eighteenth century.

The development of millennium-long hydroclimate-sensitive tree-ring records is particularly difficult in sub-Arctic in general (Linderholm et al., 2018) and, in particular, in those parts of the boreal zone that are underlain by permafrost serving as a source of additional water supply for the trees during dry summers (Sugimoto et al., 2002; Saurer et al., 2016). Although potential to develop long chronologies in the region exist (Thomsen, 2001; Agafonov et al., 2016) only a limited number of Siberian sites show statistically significant, albeit weak, correlations between tree growth and either monthly (Kirdyanov et al., 2013; Shestakova et al., 2019) or summer (Hellmann et al., 2016) precipitation or monthly SPEI Arzac et al. (2019). Not surprisingly, hydroclimate

Table 7

Climate Signal scores. Length is the period of overlap with instrumental temperature data in years. Correlation is the Pearson correlation coefficient between the tree-ring chronology and the instrumental data over the calibration period. Calibration/verification difference indicates the correlation range between different periods of overlap with instrumental data. Truncation = 0.5 if the calibration period was shortened (e.g. due to divergence), truncation = 1 if this is not the case. (For interpretation of the references to color in this table legend, the reader is referred to the Web version of this article.)

5. Climate signal					
4. Truncation					
3. Calibration/verification difference					
2. Correlation					
1. Length [yrs.]					
Upper Arkansas River Basin, USA	107	0.83	0.04	1	●
Yampa River, USA	97	0.82	0.06	1	●
Tavaputs Plateau, USA	87	0.89	0.10	1	●
Mesa Verde, USA (EW)	86	0.83	0.04	1	●
El Malpais, USA	97	0.76	0.02	1	●
Upper Klamath River Basin, USA	115	0.73	0.06	1	●
Little Snake River, USA	96	0.78	0.05	1	●
White River, USA	97	0.82	0.15	1	●
Southern Colorado Plateau, USA	98	0.77	0.11	1	●
Southern Sierra Nevada, USA	116	0.70	0.11	1	●
Bear River, USA	68	0.90	0.18	1	●
Mesa Verde, USA (LW)	86	0.65	0.02	1	●
El Malpais, USA (LW)	71	0.71	0.02	1	●
Jemez Mountains, USA	112	0.60	0.06	1	●
Atlas Mountains, Morocco	71	0.75	0.10	1	●
Central Chile	85	0.67	0.08	1	●
Northeastern Tibetan Plateau, China	55	0.84	0.14	1	●
Urgat, Mongolia	52	0.74	0.03	1	●
Heihe River Basin	49	0.74	0.01	1	●
Southerncentral England, UK	107	0.57	0.08	1	●
Mount Smolikas, Greece	54	0.69	0.04	1	●
East Anglia, UK	109	0.56	0.11	1	●
Khorgo, Mongolia	52	0.71	0.06	1	●
Mount San Gorgonio, USA	102	0.60	0.16	1	●
Southern Finland	84	0.67	0.19	1	●
Summitville, USA	115	0.47	0.06	1	●
Hexi Corridor, China	61	0.63	0.12	1	●
A'nyêmaqên, China	48	0.74	0.17	1	●
Delingha, China	46	0.63	0.06	1	●
White Mountains, USA	48	0.59	0.04	1	●
El Malpais, USA (EW)	71	0.68	0.23	1	●
Qilian Mountains, China	45	0.66	0.10	1	●
Whirlpool point, Canada	85	0.51	0.13	1	●
Lee Ferry, USA	65	0.85	0.02	1	●
Choctawhatchee River, USA (EW)	91	0.64	0.03	0.5	●
Colorado River, USA	65	0.71	0.02	1	●
Choctawhatchee River, USA (LW)	91	0.62	0.06	0.5	●
Sacramento River, USA	73	0.70	0.08	0.5	●
Georgia, USA	91	0.60	0.09	0.5	●
Barranca de Amealco, Mexico	54	0.79	0.25	0.5	●
Dulan, China	34	0.70	0.05	0.5	●
Flowerpot, Canada	115	0.50	0.15	0.5	●
Pamir-Alay Mountains, Tajikistan	54	0.69	0.21	0.5	●
Albemarle Sound, USA	89	0.57	0.22	0.5	●
Central Europe	80	0.50	0.15	0.5	●
Potomac River, USA	70	0.59	0.23	0.5	●



Class A



Class B



Class C



Class D

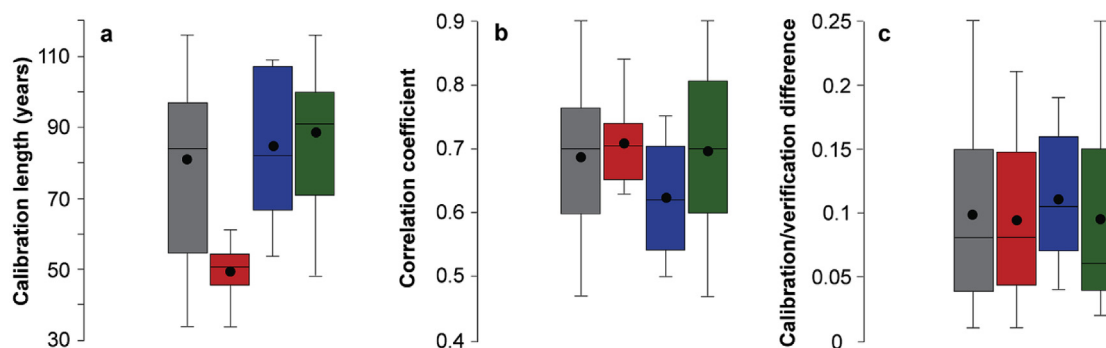


Fig. 8. Box plot figures showing the distribution of *Climate Signal* scores for all 46 reconstructions (grey), Asia (red), Europe and North Africa (blue), and North America (green) with a box drawn between the first and third quartiles, a line across the box shows the median, the black dot shows the mean, and minimum and maximum values indicated by whiskers. (a) Length of the calibration period in years. (b) Pearson correlation coefficient between the tree-ring chronology and the instrumental data over the calibration period. (c) Difference between correlation values of the calibration/verification periods.

reconstructions in the warmer and drier southern Siberia have shown greater promise (Shah et al., 2015; Belokopytova et al., 2018; Kostyakova et al., 2018). A new impetus to long hydroclimate reconstructions in the boreal zone, particular in Siberia, may be provided with the development of tree-ring stable isotope chronologies (e.g., Waterhouse et al., 2000; Kirdyanov et al., 2008; Sidorova et al., 2009, 2010, 2012; Knorre et al., 2010; Tei et al., 2013, 2015; Panyushkina et al., 2016; Shestakova et al., 2017).

The moisture-limited tree growth environments of Central Asia, the Middle East, and North Africa have a high potential to yield millennium-long hydroclimate tree-ring reconstructions but comparatively little work has so far been done in the region. However, several century long reconstructions have been developed for Turkey (D'Arrigo and Cullen, 2001; Touchan et al., 2003, 2005, 2007; Akkemik and Aras, 2005; Akkemik et al., 2005, 2008), Jordan (Touchan et al., 1999) and the Caucasus (Martin-Benito et al., 2016). For instance, Solomina et al. (2014), Seim et al. (2016a, b), Wang et al. (2017), Zhang et al. (2017), Chen et al. (2019) demonstrated the feasibility to reconstruct drought or precipitation in Central Asia. Opała-Owczarek and Niedźwiedź (2018) showed that it is possible to extend hydroclimate reconstructions for this region for the full past millennium or more. Likewise, Esper et al. (2007) successfully developed a past millennium reconstruction from the Atlas Mountains of Morocco.

Although the vast majority of existing tree-ring based hydroclimate reconstructions are from Northern Hemisphere, there are potential to develop moisture-sensitive chronologies in the Southern Hemisphere as well. Early efforts by Schulman (1956) recognized a number of South American tree species sensitive to precipitation variations, and in the 1970s the first tree-ring based estimates of past hydroclimate conditions was developed in southern South America (LaMarche, 1978; Holmes et al., 1979). Recent work includes streamflow reconstructions spanning the past four to six centuries from the sub-Antarctic (Lara et al., 2008, 2015), the temperate (Urrutia et al., 2011; Mundo et al., 2012; Muñoz et al., 2016) and the subtropical (Ferrero et al., 2015) regions along the Andes, and even longer hydroclimate reconstructions from the Andes of central Chile (Le Quesne et al., 2006, 2009; Masiokas et al., 2012) and the Bolivian Altiplano (Morales et al., 2012). Recent studies have also shown a potential in the South American tropics (Lopez et al., 2017; Granato-Souza et al., 2019), as well as Australia, although efforts in the latter region are hampered by large spatial hydroclimatic heterogeneity (Allen et al., 2019) as

well as the short temporal extension of the data (Allen et al., 2015).

4.4. Recommendations for future hydroclimate reconstructions

The six recommendations presented by Esper et al. (2016) for tree-ring based temperature reconstructions also hold true for the development of hydroclimate reconstructions: (a) preserving centennial-scale variability, using RCS detrending, for understanding low-frequency variance, (b) avoiding a strong decrease of series back in time, (c) strive for a homogeneous sample composition over time, (d) avoid too large replication and inter-series correlation changes, (e) avoid strong age curve changes over time, and (f) keep in mind that the calibration statistics may give a false impression of reconstruction skill. Based on the results from this assessment, we find it important to improve the replication in the earlier parts of the reconstructions, especially in North America, as a weak replication during medieval times precludes robust comparisons with recent hydroclimate conditions. It is equally important to include young and old trees throughout time in the chronologies to achieve a more evenly distributed age curve. The most difficult trade-off, however, is likely between achieving a high sample replication (over time) and a strong growth coherence, as the inclusion of additional sites can degrade growth coherence within a reconstruction. It appears less advisable to include more than, at most, two tree species in any reconstruction and they should ideally derive from the same genera. When tree-ring material is obtained from multiple sites, it is important that it originates from similar environments with regard to moisture stress. Whenever notable micro site conditions exist (Düthorn et al., 2015), temporal clustering of a certain micro site condition should be avoided.

For tree-ring datasets composed of relatively young trees it is essential to successfully apply RCS detrending to preserve low-frequency information. This requires a large number of raw measurement series from relatively evenly distributed tree age over time. If the biological age of measurements shows a steep increase towards the present RCS should only be applied with great caution. The use of measurement series from very old trees as an alternative to RCS detrending, at the price of a steep age curve, to preserve low-frequency variability may introduce biases from a climate signal age effect (Esper et al., 2008; Konter et al., 2016) and should be avoided if possible.

We find that a strong and stable hydroclimate signal is of far

Table 8

Ranking of the 46 tree-ring based hydroclimate reconstructions based on their *Data Homogeneity*, *Sample replication*, *Growth Coherence*, *Chronology Development*, and *Climate Signal* scores. Last column indicates which datasets are publicly available. (For interpretation of the references to color in this table legend, the reader is referred to the Web version of this article.)

	6. Data	5. Climate signal	4. Chronology development	3. Growth coherence	2. Replication	1. Homogeneity	
Khorgo, Mongolia	●	●	●	●	●	●	✓
Tavaputs Plateau, USA	●	●	●	●	●	●	✓
Uurgat, Mongolia	●	●	●	●	●	●	✓
El Malpais, USA	●	●	●	●	●	●	✓
Southern Sierra Nevada, USA	●	●	●	●	●	●	✓
Summitville, USA	●	●	●	●	●	●	✓
Bear River, USA	●	●	●	●	●	●	✓
White Mountains, USA	●	●	●	●	●	●	✓
Northeastern Tibetan Plateau, China	●	●	●	●	●	●	✓
East Anglia, UK	●	●	●	●	●	●	✓
Whirlpool point, Canada	●	●	●	●	●	●	✓
Southerncentral England, UK	●	●	●	●	●	●	✓
Hexi Corridor, China	●	●	●	●	●	●	✓
Heihe River Basin, China	●	●	●	●	●	●	✓
El Malpais, USA (LW)	●	●	●	●	●	●	✓
Upper Klamath River Basin, USA	●	●	●	●	●	●	✓
Mount Smolikas, Greece	●	●	●	●	●	●	✓
El Malpais, USA (EW)	●	●	●	●	●	●	✓
Choctawhatchee River, USA (EW)	●	●	●	●	●	●	✓
Mesa Verde, USA (EW)	●	●	●	●	●	●	✓
Southern Finland	●	●	●	●	●	●	✓
Atlas Mountains, Morocco	●	●	●	●	●	●	✓
Anyêm aqên, China	●	●	●	●	●	●	✓
Delingha, China	●	●	●	●	●	●	✓
Upper Arkansas River Basin, USA	●	●	●	●	●	●	✓
Central Europe	●	●	●	●	●	●	✓
Mount San Gorgonio	●	●	●	●	●	●	✓
Southern Colorado Plateau, USA	●	●	●	●	●	●	✓
Flowerpot, Canada	●	●	●	●	●	●	✓
Mesa Verde, USA (LW)	●	●	●	●	●	●	✓
Central Chile	●	●	●	●	●	●	✓
Barranca de Amealco, Mexico	●	●	●	●	●	●	✓
Choctawhatchee River, USA (LW)	●	●	●	●	●	●	✓
Dulan, China	●	●	●	●	●	●	✓
Jemez Mountains, USA	●	●	●	●	●	●	✓
Sacramento River, USA	●	●	●	●	●	●	✓
Little Snake River, USA	●	●	●	●	●	●	✓
Yampa River, USA	●	●	●	●	●	●	✓
Potomac River, USA	●	●	●	●	●	●	✓
Albemarle Sound, USA	●	●	●	●	●	●	✓
White River, USA	●	●	●	●	●	●	✓
Qilian Mountains, China	●	●	●	●	●	●	✓
Lee Ferry, USA	●	●	●	●	●	●	✓
Pamir-Alay Mountains, Tajikistan	●	●	●	●	●	●	✓
Colorado River, USA	●	●	●	●	●	●	✓
Georgia, USA	●	●	●	●	●	●	✓

● Class A ● Class B ● Class C ● Class D

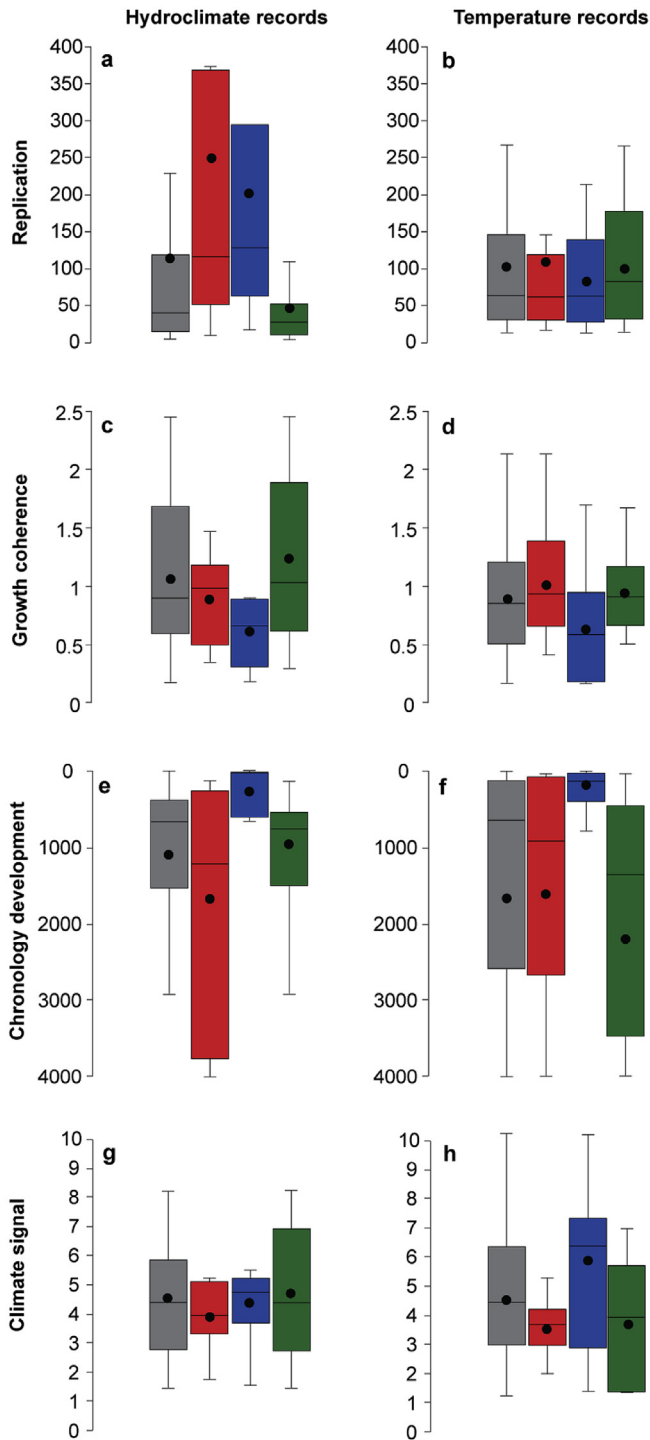


Fig. 9. Comparison of Sample Replication, Growth Coherence, Chronology Development, and Climate Signal scores for the 46 hydroclimate reconstructions in this study and the 39 temperature reconstructions from Esper et al. (2016), with a box drawn between the first and third quartiles, a line across the box shows the median, the black dot shows the mean, and minimum and maximum values indicated by whiskers. All reconstructions (grey), Asia (red), Europe and North Africa (blue), and North America (green). (a) Sample Replication scores for hydroclimate reconstructions. (b) Sample Replication scores for temperature reconstructions. (c) Growth Coherence scores for hydroclimate reconstructions. (d) Growth Coherence scores for temperature reconstructions. (e) Chronology Development scores for hydroclimate reconstructions. (f) Chronology Development scores for temperature reconstructions. (g) Climate Signal scores for hydroclimate reconstructions. (h) Climate Signal scores for temperature reconstructions.

greater importance than having a long calibration period. This implies that it is fully feasible to develop well-verified tree-ring based hydroclimate also from regions with short instrumental measurements. Moreover, it needs to be kept in mind that the calibration statistics obtained, regardless of the length of instrumental measurements, typically are optimistic estimates in the sense that the inter-series correlation as well as sample replication typically decreases back in time. If the calibration had been conducted on a less replicated part of the reconstruction, with lower inter-series correlation values, the correlation values would in most cases have been lower. Tests including artificially reduced-sample chronologies (Esper et al., 2012) are thus recommended.

5. Conclusions

Following a scheme developed by Esper et al. (2016) for temperature reconstructions, we assessed and ranked 46 millennium-long tree-ring based hydroclimate reconstructions. This scoring considers: *Data Homogeneity*, *Sample Replication*, *Growth Coherence*, *Chronology Development*, and *Climate Signal* (Fig. 10). Most of these characteristics, with the exception of *Climate Signal*, are rarely or ever considered outside the dendrochronological community, but impacts paleoclimate reconstruction–model simulation comparison studies. Our assessment will guide secondary users of tree-ring based hydroclimate reconstructions by providing information on the strength and limitations of the individual records beyond their simple correlation with instrumental data. Moreover, we hope these results will advance future work on developing new tree-ring based hydroclimate reconstructions or improving and extending the existing ones.

The ranking scores produced for each of the five evaluation categories represent an attempt at objectively identifying suitable and less suitable hydroclimate reconstructions to use for different purposes. For example, in a study of short-term hydroclimate impacts following large volcanic eruptions, long-term trends and variations are less important in a particular reconstruction. On the other hand, if the purpose is to compare the average hydroclimate conditions during medieval times with those of today, it is advisable to only consider reconstructions that realistically retain low-frequency variability. We conclude that the same ranking implications and related recommendations for tree-ring based temperature reconstructions by Esper et al. (2016) are also valid for tree-ring based hydroclimate reconstructions (see section 4.2).

The systematic assessment of 46 tree-ring based hydroclimate reconstructions, covering the past millennium, permitted ranking them into four groups (class A to class D) for each of the five categories *Data Homogeneity*, *Sample Replication*, *Growth Coherence*, *Chronology Development*, and *Climate Signal*. All reconstructions have their various strengths and weaknesses – and no reconstruction ranked A or D in all five categories – but there are some reconstructions that consistently performed high: Khorgo (Hessl et al., 2018), the Northeastern Tibetan Plateau (Yang et al., 2014), and Uurgat (Hessl et al., 2018) from Asia; East Anglia (Cooper et al., 2013) and Southerncentral England (Wilson et al., 2013) from Europe; Tavaputs Plateau (Knight et al., 2010), El Malpais (Grissino-Mayer, 1995), Southern Sierra Nevada (Graumlich, 1993), Summitville (Routson et al., 2011), and Bear River (DeRose et al., 2015) from North America. Though it is our goal to provide evaluations that will assist investigators in making informed selections for their purposes, we at the same time recognize that all the reconstructions contain valuable information depending on the questions asked of them.

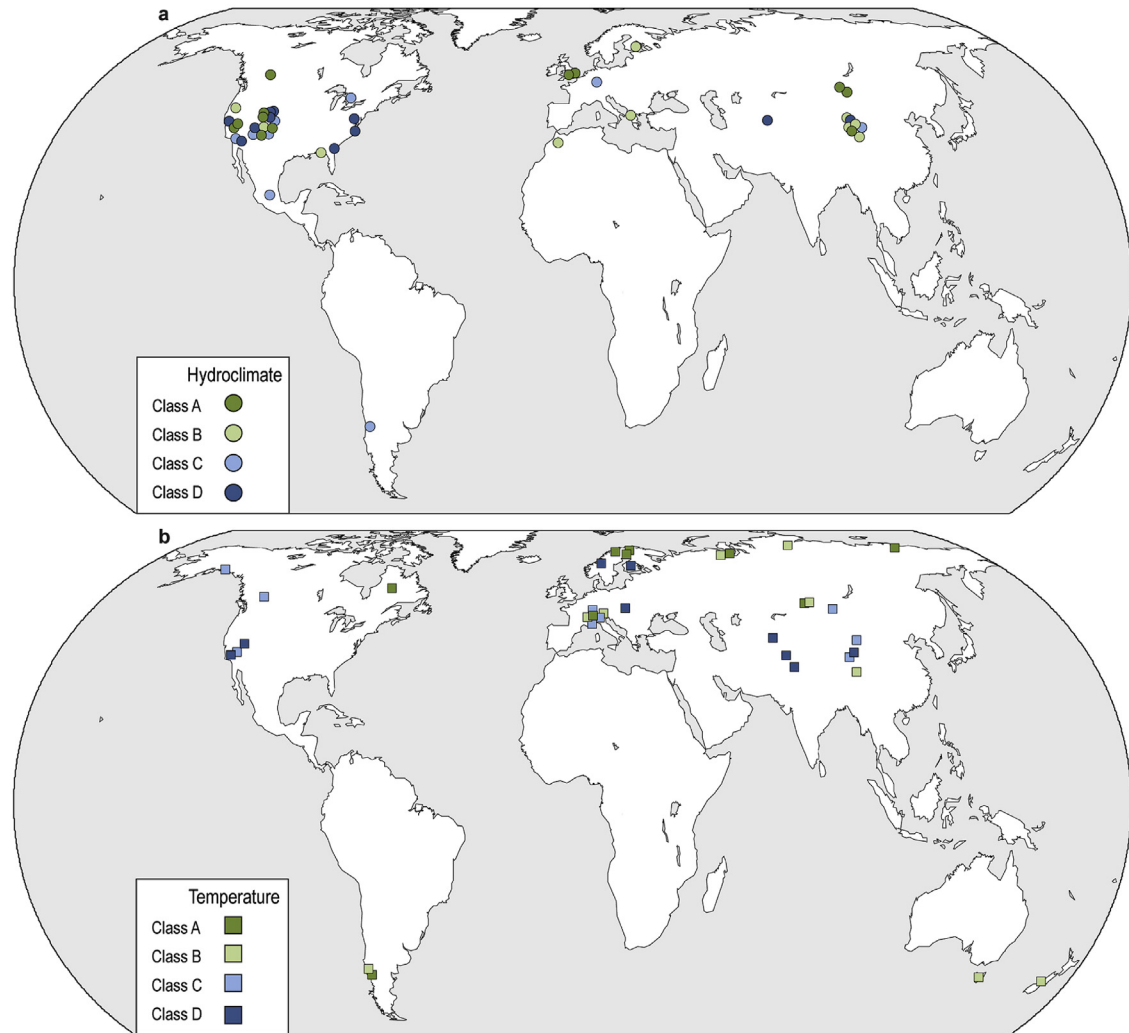


Fig. 10. Maps showing (a) the distributions of the 46 tree-ring based hydroclimate reconstructions (this study), and (b) the 39 temperature reconstructions (Esper et al., 2016) divided into four ranking classes A to D.

Acknowledgements

We are grateful to all colleagues for sharing and providing their tree-ring chronologies and measurement series. F.C.L. was supported by the Swedish Research Council (Vetenskapsrådet, grant 2018-01272), A.S. by the German Research Foundation (Deutsche Forschungsgemeinschaft, SE 2802/1-1), U.B. by the Czech Republic Grant Agency project no. 17-22102S, M.H. by the Alexander von Humboldt Foundation, J.L., L.S. and B.Y. by the Belmont Forum and JPI-Climate, Collaborative Research Action “INTEGRATE: An integrated data–model study of interactions between tropical monsoons and extratropical climate variability and extremes” (BMBF grant 01LP1612A; NERC grant NE/P006809/1; NSFC grant 41661144008), K.S. by FORMAS (grant 2014-723) and the Swiss National Science Foundation SNSF (project XELLCLIM no. 200021-182398), J.E. by the German Research Foundation (Deutsche Forschungsgemeinschaft, grants Inst 247/665-1 FUGG and ES 161/9-1). F.C.L. acknowledges a longer stay as Visiting Scholar at the Department of Geography, University of Cambridge, allowing time and inspiration to pursue this study. All reconstructions, with the data in the public domain, and their corresponding scores are provided at www.blogs.uni-mainz.de/fb09climatology.

References

- Agafonov, L.I., Meko, D.M., Panyushkina, I.P., 2016. Reconstruction of Ob River, Russia, discharge from ring widths of floodplain trees. *J. Hydrol.* 543, 198–207. <https://doi.org/10.1016/j.jhydrol.2016.09.031>.
- Akkemik, Ü., Aras, A., 2005. Reconstruction (1689–1994 AD) of April–August precipitation in the southern part of central Turkey. *Int. J. Climatol.* 25, 537–548. <https://doi.org/10.1002/joc.1145>.
- Akkemik, Ü., Dagdeviren, N., Aras, A., 2005. A preliminary reconstruction (A.D. 1635–2000) of spring precipitation using oak tree rings in the Western Black Sea Region of Turkey. *Int. J. Biometeorol.* 49, 297–302. <https://doi.org/10.1007/s00484-004-0249-8>.
- Akkemik, Ü., D'Arrigo, R., Cherubini, P., Köse, N., Jacoby, G.C., 2008. Tree-ring reconstructions of precipitation and streamflow for north-western Turkey. *Int. J. Climatol.* 28, 173–183. <https://doi.org/10.1002/joc.1522>.
- Allen, K.J., Nichols, S.C., Evans, R., Cook, E.R., Allie, S., Carson, G., Ling, F., Baker, P.J., 2015. Preliminary December–January inflow and streamflow reconstructions from tree rings for western Tasmania, southeastern Australia. *Water Resour. Res.* 51, 5487–5503. <https://doi.org/10.1002/2015WR017062>.
- Allen, K.J., Brookhouse, M., French, B.J., Nichols, S.C., Dahl, B., Norrie, D., Prior, L.D., Palmer, J.G., Bowman, D.J.M.S., 2019. Two climate-sensitive tree-ring chronologies from Arnhem Land, monsoonal Australia. *Austral Ecol.* 44, 581–596. <https://doi.org/10.1111/aec.12699>.
- Anchukaitis, K.J., 2017. Tree rings reveal climate change past, present, and future. *Proc. Am. Philos. Soc.* 161, 244–263.
- Arzac, A., Popkova, M., Anarbekova, A., Olano, J., Gutiérrez, E., Nikolaev, A., Shishov, V., 2019. Increasing radial and latewood growth rates of *Larix cajanderi* Mayr. and *Pinus sylvestris* L. in the continuous permafrost zone in Central

- 0959683610391312.
- Duffy, J.E., McCarroll, D., Loader, N.J., Young, G.H.F., Davies, D., Miles, D., Bronk Ramsey, C., 2019. Absence of age-related trends in stable oxygen isotope ratios from oak tree rings. *Glob. Biogeochem. Cycles* 33, 841–848. <https://doi.org/10.1029/2019GB006195>.
- Düthorn, E., Schneider, L., Konter, O., Schön, P., Timonen, M., Esper, J., 2015. On the hidden significance of differing micro-sites in dendroclimatology. *Silva Fenn.* 49, 1220. <https://doi.org/10.14214/sf.1220>.
- D'Arrigo, R., Cullen, H., 2001. A 350-year (AD 1628–1980) reconstruction of Turkish precipitation. *Dendrochronologia* 19, 169–177.
- D'Arrigo, R., Wilson, R., Liepert, B., Cherubini, P., 2008. On the 'divergence problem' in northern forests: a review of the tree-ring evidence and possible causes. *Glob. Planet. Chang.* 60, 289–305. <https://doi.org/10.1016/j.gloplacha.2007.03.004>.
- Edwards, T.W., Birks, S.J., Luckman, B.H., MacDonald, G.M., 2008. Climatic and hydrologic variability during the past millennium in the eastern Rocky Mountains and northern Great Plains of western Canada. *Quat. Res.* 70, 188–197. <https://doi.org/10.1016/j.yqres.2008.04.013>.
- Edwards, T.W.D., Hammarlund, D., Newton, B.W., Sjolte, J., Linderson, H., Sturm, C., St Amour, N.A., Bailey, J.N.L., Nilsson, A.L., 2017. Seasonal variability in Northern Hemisphere atmospheric circulation during the Medieval Climate Anomaly and the Little Ice Age. *Quat. Sci. Rev.* 165, 102–110. <https://doi.org/10.1016/j.quascirev.2017.04.018>.
- Esper, J., Cook, E.R., Krusic, P.J., Peters, K., Schweingruber, F.H., 2003. Tests of the RCS method for preserving low-frequency variability in long tree-ring chronologies. *Tree-Ring Res.* 59, 81–98.
- Esper, J., Frank, D., Verstege, A., Luterbacher, J., Xoplaki, E., 2007. Long-term drought severity variations in Morocco. *Geophys. Res. Lett.* 34, L17702. <https://doi.org/10.1029/2007gl030844>.
- Esper, J., Niederer, R., Bebi, P., Frank, D.C., 2008. Climate signal age effects – evidence from young and old trees in the Swiss Engadin. *For. Ecol. Manag.* 255, 3783–3789. <https://doi.org/10.1016/j.foreco.2008.03.015>.
- Esper, J., Frank, D.C., Timonen, M., Zorita, E., Wilson, R.J.S., Luterbacher, J., Holzkämper, S., Fischer, N., Wagner, S., Nievergelt, D., Verstege, A., Büntgen, U., 2012. Orbital forcing of tree-ring data. *Nat. Clim. Chang.* 2, 862–866. <https://doi.org/10.1038/nclimate1589>.
- Esper, J., Krusic, P.J., Ljungqvist, F.C., Luterbacher, J., Carrer, M., Cook, E., Davi, N.K., Hartl-Meier, C., Kiryanov, A., Konter, O., Myglan, V., Timonen, M., Treydte, K., Trouet, V., Villalba, R., Yang, B., Büntgen, U., 2016. Ranking of tree-ring based temperature reconstructions of the past millennium. *Quat. Sci. Rev.* 145, 134–151. <https://doi.org/10.1016/j.quascirev.2016.05.009>.
- Esper, J., St George, S., Anchukaitis, K., D'Arrigo, R., Ljungqvist, F.C., Luterbacher, J., Schneider, L., Stoffel, M., Wilson, R., Büntgen, U., 2018. Large-scale, millennial-length temperature reconstructions from tree-rings. *Dendrochronologia* 50, 81–90. <https://doi.org/10.1016/j.dendro.2018.06.001>.
- Feng, S., Hu, Q., Wu, Q., Mann, M.E., 2013. A gridded reconstruction of warm season precipitation for Asia spanning the past half millennium. *J. Clim.* 26, 2192–2204. <https://doi.org/10.1175/JCLI-D-12-00099.1>.
- Ferrero, M.E., Villalba, R., De Membrillo, M., Ferri Hidalgo, L., Luckman, B.H., 2015. Tree-ring based reconstruction of Río Bermejo streamflow in subtropical South America. *J. Hydrol.* 525, 572–584. <https://doi.org/10.1016/j.jhydrol.2015.04.004>.
- Field, C.B., Barros, V.R., Mach, K., Mastrandrea, M., Bilir, E., Chatterjee, M., Ebi, K.L., Estrada, Y.O., Genova, R.C., Girma, B., Kissel, E.S., Levy, A.N., MacCracken, S., Mastrandrea, P.R., White, L.L., 2014. Climate change 2014: impacts, adaptation, and vulnerability. Part A: global and sectoral aspects. In: *Contribution of Working Group II to the Fifth Assessment Report of the Intergovernmental Panel on Climate Change*. Cambridge University Press, Cambridge, p. 1132.
- Frank, D., Esper, J., Zorita, E., Wilson, R., 2010. A noodle, hockey stick, and spaghetti plate: a perspective on high-resolution paleoclimatology. *Wiley Interdiscip. Rev. Clim. Change* 1, 507–516. <https://doi.org/10.1002/wcc.53>.
- Franke, J., Frank, D., Raible, C.C., Esper, J., Brönnimann, S., 2013. Spectral biases in tree-ring climate proxies. *Nat. Clim. Chang.* 3, 360–364. <https://doi.org/10.1038/nclimate1816>.
- Fritts, H.C., 1976. *Tree Rings and Climate*. Academic Press, London.
- Garreaud, R., Alvarez-Garretón, C., Barichivich, J., Boisier, J.P., Christie, D., Galleguillos, M., Zambrano-Bigiarini, M., 2017. The 2010–2015 mega drought in central Chile: impacts on regional hydroclimate and vegetation. *Hydrol. Earth Syst. Sci.* 21, 6307–6327. <https://doi.org/10.5194/hess-21-6307-2017>.
- Gou, X., Deng, Y., Chen, F., Yang, M., Fang, K., Gao, L., Yang, T., Zhang, F., 2010. Tree ring based streamflow reconstruction for the Upper Yellow River over the past 1234 years. *Sci. Bull.* 55, 4179–4186. <https://doi.org/10.1007/s11434-010-4215-z>.
- Granato-Souza, D., Stahle, D.W., Barbosa, A.C., Feng, S., Torbenson, M.C.A., de Assis Pereira, G., Schöngart, J., Barbosa, J.P., Griffin, D., 2019. Tree rings and rainfall in the equatorial Amazon. *Clim. Dyn.* 52, 1857–1869. <https://doi.org/10.1007/s00382-018-4227-y>.
- Graumlich, L.J., 1993. A 1000-year record of temperature and precipitation in the Sierra Nevada. *Quat. Res.* 39, 249–255. <https://doi.org/10.1006/qres.1993.1029>.
- Gray, S.T., Lukas, J.J., Woodhouse, C.A., 2011. Millennial-length records of streamflow from three major Upper Colorado River tributaries. *J. Am. Water Resour. Assoc.* 47, 702–712. <https://doi.org/10.1111/j.1752-1688.2011.00535.x>.
- Griessinger, J., Bräuning, A., Helle, G., Hochreuther, P., Schleser, G., 2017. Late Holocene relative humidity history on the southeastern Tibetan Plateau inferred from a tree-ring $\delta^{18}\text{O}$ record: recent decrease and conditions during the last 1500 years. *Quat. Int.* 430, 52–59. <https://doi.org/10.1016/j.quaint.2016.02.011>.
- Grissino-Mayer, H.D., 1993. An updated list of species used in tree-ring research. *Tree-Ring Res.* 53, 17–43.
- Grissino-Mayer, H.D., 1995. *Tree-ring Reconstructions of Climate and Fire History at El Malpais National Monument, New Mexico*. PhD dissertation. The University of Arizona.
- Grissino-Mayer, H.D., Fritts, H.C., 1997. The International Tree-Ring Data Bank: an enhanced global database serving the global scientific community. *Holocene* 7, 235–238. <https://doi.org/10.1177/095968369700700212>.
- Harris, I., Jones, P.D., Osborn, T.J., Lister, D.H., 2014. Updated high-resolution grids of monthly climatic observations – the CRU TS3.10 dataset. *Int. J. Climatol.* 34, 623–642. <https://doi.org/10.1002/joc.3711>.
- Hawley, F., Clark, N.M., 1940. Trees do not lie! *Am. For.* 46, 66–68.
- He, M., Yang, B., Bräuning, A., Rossi, S., Ljungqvist, F.C., Shishov, V., Griessinger, J., Wang, J., Liu, J., Qin, C., 2019. Recent advances in dendroclimatology in China. *Earth Sci. Rev.* 194, 521–535. <https://doi.org/10.1016/j.earscirev.2019.02.012>.
- Helama, S., Lindholm, M., 2003. Droughts and rainfall in south eastern Finland since AD 874, inferred from Scots pine tree-rings. *Boreal Environ. Res.* 8, 171–183.
- Helama, S., Meriläinen, J., Tuomenvirta, H., 2009. Multicentennial megadrought in northern Europe coincided with a global El Niño–Southern Oscillation drought pattern during the Medieval Climate Anomaly. *Geology* 37, 175–178. <https://doi.org/10.1130/G25329A.1>.
- Helama, S., Fauria, M.M., Mielikäinen, K., Timonen, M., Eronen, M., 2010. Sub-Milankovitch solar forcing of past climates: mid and late Holocene perspectives. *GSA Bull.* 122, 1981–1988. <https://doi.org/10.1130/B30088.1>.
- Hellmann, L., Agafonov, L., Ljungqvist, F.C., Churakova (Sidorova), O., Düthorn, E., Esper, J., Hülsmann, L., Kiryanov, A.V., Moiseev, P., Myglan, V.S., Nikolaev, A.N., Reinig, F., Schweingruber, F.H., Solomina, O., Tegel, W., Büntgen, U., 2016. Diverse growth trends and climate responses across Eurasia's boreal forest. *Environ. Res. Lett.* 11, 074021. <https://doi.org/10.1088/1748-9326/11/7/074021>.
- Hessl, A.E., Anchukaitis, K.J., Jelsema, C., Cook, B., Byambasuren, O., Leland, C., Nachin, B., Pederson, N., Tian, H., Hayles, L.A., 2018. Past and future drought in Mongolia. *Sci. Adv.* 4, e1701832. <https://doi.org/10.1126/sciadv.1701832>.
- Ho, M., Lall, U., Cook, E.R., 2016. Can a paleodrought record be used to reconstruct streamflow? a case study for the Missouri River Basin. *Water Resour. Res.* 52, 5195–5212. <https://doi.org/10.1002/2015WR018444>.
- Hobbins, M.T., Dai, A., Roderick, M.L., Farquhar, G.D., 2008. Revisiting potential evapotranspiration parameterizations as drivers of long-term water balance trends. *Geophys. Res. Lett.* 35, L12403. <https://doi.org/10.1029/2008GL033840>.
- Hofstra, N., New, M., 2009. Spatial variability in correlation decay distance and influence on angular-distance weighting interpolation of daily precipitation over Europe. *Int. J. Climatol.* 29, 1872–1880. <https://doi.org/10.1002/joc.1819>.
- Holmes, R.L., Stockton, C.W., LaMarche, V.C., 1979. Extension of riverflow records in Argentina from long tree-ring chronologies. *Water Resour. Bull.* 15, 1081–1085. <https://doi.org/10.1111/j.1752-1688.1979.tb01086.x>.
- Hughes, M.K., Graumlich, L.J., 1996. Multimillennial dendroclimatic studies from the western United States. In: *Climatic Variations and Forcing Mechanisms of the Last 2000 Years*. Springer, pp. 109–124.
- Hurst, H.E., 1951. Long term storage capacities of reservoirs. *Trans. Am. Soc. Civ. Eng.* 116, 776–808.
- Jacobi, J., Perrone, D., Lyons Duncan, L., Hornberger, G., 2013. A tool for calculating the Palmer drought indices. *Water Resour. Res.* 49, 6086–6089. <https://doi.org/10.1002/wrcr.20342>.
- Jones, P.D., Osborn, T.J., Briffa, K.R., 1997. Estimating sampling errors in large-scale temperature averages. *J. Clim.* 10, 2548–2568. [https://doi.org/10.1175/1520-0442\(1997\)010<2548:ESEILS>2.0.CO;2](https://doi.org/10.1175/1520-0442(1997)010<2548:ESEILS>2.0.CO;2).
- Jönsson, K., Nilsson, C., 2009. Scots pine (*Pinus sylvestris* L.) on shingle fields: a dendrochronologic reconstruction of early summer precipitation in mid-east Sweden. *J. Clim.* 22, 4710–4722. <https://doi.org/10.1175/2009JCLI2401.1>.
- Karl, T.R., 1986. The sensitivity of the Palmer Drought Severity Index and Palmer's Z-Index to their calibration coefficients including potential evapotranspiration. *J. Clim. Appl. Meteorol.* 25, 77–86. [https://doi.org/10.1175/1520-0450\(1986\)025<0077:TSOTPD>2.0.CO;2](https://doi.org/10.1175/1520-0450(1986)025<0077:TSOTPD>2.0.CO;2).
- Keyantash, J., Dracup, J.A., 2002. The quantification of drought: an evaluation of drought indices. *Bull. Am. Meteorol. Soc.* 83, 1167–1180. <https://doi.org/10.1175/1520-0477-83.8.1167>.
- Kiryanov, A.V., Treydte, K.S., Nikolaev, A., Helle, G., Schleser, G.H., 2008. Climate signals in tree-ring width, wood density and $\delta^{13}\text{C}$ from larches in Eastern Siberia (Russia). *Chem. Geol.* 252, 31–41. <https://doi.org/10.1016/j.chemgeo.2008.01.023>.
- Kiryanov, A.V., Prokushkin, A.S., Tabakova, M.A., 2013. Tree-ring growth of Gmelin larch under contrasting local conditions in the north of Central Siberia. *Dendrochronologia* 31, 114–119. <https://doi.org/10.1016/j.dendro.2012.10.003>.
- Klippel, L., Krusic, P.J., Brandes, R., Hartl, C., Belmecheri, S., Dienst, M., Esper, J., 2018. A 1286-year hydro-climate reconstruction for the Balkan Peninsula. *Boreas* 47, 1218–1229. <https://doi.org/10.1111/bor.12320>.
- Knight, T.A., Meko, D.M., Baisan, C.H., 2010. A bimillennial-length tree-ring reconstruction of precipitation for the Tavaputs Plateau, Northeastern Utah. *Quat. Res.* 73, 107–117. <https://doi.org/10.1016/j.yqres.2009.08.002>.
- Knorre, A.A., Siegwolf, R.T.W., Saurer, M., Sidorova, O.V., Vaganov, E.A., Kiryanov, A.V., 2010. Twentieth century trends in tree ring stable isotopes ($\delta^{13}\text{C}$ and $\delta^{18}\text{O}$) of *Larix sibirica* under dry conditions in the forest steppe in Siberia. *J. Geophys. Res.: Biogeosciences* 115, G03002. <https://doi.org/10.1029/2009JG000930>.
- Konter, O., Büntgen, U., Carrer, M., Timonen, M., Esper, J., 2016. Climate signal age effects in boreal tree-rings: lessons to be learned for paleoclimatic

- reconstructions. *Quat. Sci. Rev.* 142, 164–172. <https://doi.org/10.1016/j.quascirev.2016.04.020>.
- Kostyakova, T.V., Touchan, R., Babushkina, E.A., Belokopytova, L.V., 2018. Precipitation reconstruction for the Khakassia region, Siberia, from tree rings. *Holocene* 28, 377–385. <https://doi.org/10.1177/0959683617729450>.
- Kress, A., Hangartner, S., Bugmann, H., Büntgen, U., Frank, D.C., Leuenberger, M., Siegwolf, R.T.W., Saurer, M., 2014. Swiss tree-rings reveal warm and wet summers during medieval times. *Geophys. Res. Lett.* 41, 1732–1737. <https://doi.org/10.1002/2013GL059081>.
- LaMarche, V.C., 1978. Tree-ring evidence of past climatic variability. *Nature* 276, 334–338. <https://doi.org/10.1038/276334a0>.
- Lara, A., Villalba, R., Urrutia, R., 2008. A 400-year tree-ring record of the Puelo River summer-fall streamflow in the Valdivian Rainforest eco-region, Chile. *Clim. Change* 86, 331–356. <https://doi.org/10.1007/s10584-007-9287-7>.
- Lara, A., Bahamondez, A., González-Reyes, A., Muñoz, A.A., Cuq, E., Ruiz-Gómez, C., 2015. Reconstructing streamflow variation of the Baker River from tree-rings in Northern Patagonia since 1765. *J. Hydrol.* 529, 511–523. <https://doi.org/10.1016/j.jhydrol.2014.12.007>.
- Le Quesne, C., Stahle, D.W., Cleaveland, M.K., Therrell, M.D., Aravena, J.C., Barichivich, J., 2006. Ancient *Austrocedrus* tree-ring chronologies used to reconstruct central Chile precipitation variability from A.D. 1200 to 2000. *J. Clim.* 19, 5731–5744. <https://doi.org/10.1175/JCLI3935.1>.
- Le Quesne, C., Acuña, C., Boninsegna, J.A., Rivera, A., Barichivich, J., 2009. Long-term glacier variations in the Central Andes of Argentina and Chile, inferred from historical records and tree-ring reconstructed precipitation. *Palaeogeogr. Palaeoclimatol. Palaeoecol.* 281, 334–344. <https://doi.org/10.1016/j.palaeo.2009.07.020>.
- Lehner, F., Coats, S., Stocker, T.F., Pendergrass, A.G., Sanderson, B.M., Raible, C.C., Smerdon, J.E., 2017. Projected drought risk in 1.5°C and 2°C warmer climates. *Geophys. Res. Lett.* 44, 7419–7428. <https://doi.org/10.1002/2017GL074117>.
- Linderholm, H.W., Linderholm, K., 2004. Age-dependent climate sensitivity of *Pinus sylvestris* L. in the central Scandinavian mountains. *Boreal Environ. Res.* 9, 307–317.
- Linderholm, H.W., Niklasson, M., Molin, T., 2004. Summer moisture variability in East Central Sweden since the mid-eighteenth century recorded in tree rings. *Geogr. Ann.* 86A, 277–287. <https://doi.org/10.1111/j.0435-3676.2004.00231.x>.
- Linderholm, H.W., Nicolle, M., Francus, P., Gajewski, K., Helama, S., Korhola, A., Solomina, O., Yu, Z., Zhang, P., D'Andrea, W.J., Debret, M., Divine, D.V., Gunnarsson, B.E., Loader, N.J., Massei, N., Seftigen, K., Thomas, E.K., Werner, J., Andersson, S., Berntsson, A., Luoto, T.P., Nevalainen, L., Saarni, S., Välranta, M., 2018. Arctic hydroclimate variability during the last 2000 years: current understanding and research challenges. *Clim. Past* 14, 473–514. <https://doi.org/10.5194/cp-14-473-2018>.
- Liu, Y., An, Z.S., Ma, H.Z., Cai, Q.F., Liu, Z.Y., Kutzbach, J.K., Shi, J.F., Song, H.M., Sun, J.Y., Yi, L., Li, Q., Yang, Y.K., Wang, L., 2006. Precipitation variation in the north-eastern Tibetan Plateau recorded by the tree rings since 850 AD and its relevance to the Northern Hemisphere temperature. *Sci. China Earth Sci.* 49, 408–420. <https://doi.org/10.1007/s11430-006-0408-3>.
- Liu, J., Yang, B., Lindenmayer, D.B., 2019. The oldest trees in China and where to find them. *Front. Ecol. Environ.* 17, 319–322. <https://doi.org/10.1002/fee.2046>.
- Ljungqvist, F.C., Krusic, P.J., Sundqvist, H.S., Zorita, E., Brattström, G., Frank, D., 2016. Northern Hemisphere hydroclimate variability over the past twelve centuries. *Nature* 532, 94–98. <https://doi.org/10.1038/nature17418>.
- Ljungqvist, F.C., Seim, A., Krusic, P.J., González-Rouco, J.F., Werner, J.P., Cook, E.R., Zorita, E., Luterbacher, J., Xoplaki, E., Destouni, G., Bustamante, E.G., Aguilar, C.A.M., Seftigen, K., Wang, J., Gagen, M.H., Fleitmann, D., Solomina, O., Esper, J., Büntgen, U., 2019. Summer temperature and drought co-variability across Europe since 850 CE. *Environ. Res. Lett.* 14, 084015. <https://doi.org/10.1088/1748-9326/ab2c7e>.
- Lopez, L., Stahle, D., Villalba, R., Torbenson, M., Feng, S., Cook, E., 2017. Tree ring reconstructed rainfall over the southern Amazon Basin. *Geophys. Res. Lett.* 44, 7410–7418. <https://doi.org/10.1002/2017GL073363>.
- MacDonald, G.M., 2007. Severe and sustained drought in southern California and the West: present conditions and insights from the past on causes and impacts. *Quat. Int.* 173–174, 87–100. <https://doi.org/10.1016/j.quaint.2007.03.012>.
- MacDonald, G.M., Case, R.A., 2005. Variations in the Pacific decadal oscillation over the past millennium. *Geophys. Res. Lett.* 32, L08703. <https://doi.org/10.1029/2005GL02478>.
- MacDonald, G.M., Kremenetski, K.V., Hidalgo, H., 2008. Southern California and the perfect drought: simultaneous prolonged drought in southern California and the Sacramento and Colorado river systems. *Quat. Int.* 188, 11–23. <https://doi.org/10.1016/j.quaint.2007.06.027>.
- Malevich, S.B., Woodhouse, C.A., Meko, D.M., 2013. Tree-ring reconstructed hydroclimate of the Upper Klamath basin. *J. Hydrol.* 495, 13–22. <https://doi.org/10.1016/j.jhydrol.2013.04.048>.
- Markonis, Y., Koutsoyiannis, D., 2016. Scale-dependence of persistence in precipitation records. *Nat. Clim. Chang.* 6, 399–401. <https://doi.org/10.1038/nclimate2894>.
- Martin-Benito, D., Ummenhofer, C.C., Köse, N., Güner, H.T., Pederson, N., 2016. Tree-ring reconstructed May–June precipitation in the Caucasus since 1752 CE. *Clim. Dyn.* 47, 3011–3027. <https://doi.org/10.1007/s00382-016-3010-1>.
- Marvel, K., Cook, B.I., Bonfils, C.J.W., Durack, P.J., Smerdon, J.E., Williams, A.P., 2019. Twentieth-century hydroclimate changes consistent with human influence. *Nature* 569, 59–65. <https://doi.org/10.1038/s41586-019-1149-8>.
- Masiokas, M.H., Villalba, R., Christie, D.A., Betman, E., Luckman, B.H., Le Quesne, C., Prieto, M.R., Mauget, S., 2012. Snowpack variations since AD 1150 in the Andes of Chile and Argentina (30°–37°S) inferred from rainfall, tree-ring and documentary records. *J. Geophys. Res.* 117, D05112. <https://doi.org/10.1029/2011JD016748>.
- Masson-Delmotte, V., Schulz, M., Abe-Ouchi, A., Beer, J., Ganopolski, A., González-Rouco, J.F., Jansen, E., Lambeck, K., Luterbacher, J., Naish, T., Osborn, T.J., Otto-Bliesner, B.L., Quinn, T.M., Ramesh, R., Rojas, M., Shao, X., Timmermann, A., 2013. Information from paleoclimatic archives. In: Stocker, T.F., Qin, D., Plattner, G.-K., Tignor, M., Allen, S.K., Boschung, J., Nauels, A., Xia, Y., Bex, V., Midgley, P.M. (Eds.), 2013. *Climate Change 2013: the Physical Science Basis. Contribution of Working Group 1 to the Fifth Assessment Report of the Intergovernmental Panel on Climate Change*. Cambridge University Press, Cambridge, pp. 383–464. <https://doi.org/10.1017/CBO9781107415324.013>.
- Matskovsky, V., 2016. Climatic signal in tree-ring width chronologies of conifers in European Russia. *Int. J. Climatol.* 36, 3398–3406. <https://doi.org/10.1002/joc.4563>.
- Matskovsky, V., Dolgova, E., Lomakin, N., Matveev, S., 2017. Dendroclimatology and historical climatology of Voronezh region, European Russia, since 1790s. *Int. J. Climatol.* 37, 3057–3066. <https://doi.org/10.1002/joc.4896>.
- Maxwell, R.S., Hessl, A.E., Cook, E.R., Pederson, N., 2011. A multispecies tree ring reconstruction of Potomac River streamflow (950–2001). *Water Resour. Res.* 47, W05512. <https://doi.org/10.1029/2010WR010019>.
- McKee, T.B., Doesken, N.J., Kliest, J., 1993. The relationship of drought frequency and duration to time scales. In: *Proceedings of the 8th Conference of Applied Climatology*, 17–22 January, Anaheim, CA. American Meteorological Society, Boston, MA, pp. 179–184.
- Meko, D.M., Stockton, C.W., Boggess, W.R., 1980. A tree ring reconstruction of drought in southern California. *Water Resour. Bull.* 16, 594–600.
- Meko, D.M., Woodhouse, C.A., Baisan, C.A., Knight, T., Lukas, J.J., Hughes, M.K., Salzer, M.W., 2007. Medieval drought in the upper Colorado River Basin. *Geophys. Res. Lett.* 34. <https://doi.org/10.1029/2007GL029988>.
- Melvin, T.M., Grudd, H., Briffa, K.R., 2013. Potential bias in ‘updating’ tree-ring chronologies using Regional Curve Standardization: Re-processing the Torneatrask density and ring-width data. *Holocene* 23, 364–373. <https://doi.org/10.1177/0959683612460791>.
- Morales, M.S., Christie, D.A., Villalba, R., Argollo, J., Pacajes, J., Silva, J.S., Alvarez, C.A., Llacabure, J.C., Soliz Gamboa, C., 2012. Precipitation changes in the South American Altiplano since 1300 AD reconstructed by tree-rings. *Clim. Past* 8, 653–666. <https://doi.org/10.5194/cp-8-653-2012>.
- Mundo, I.A., Masiokas, M.H., Villalba, R., Morales, M.S., Neukom, R., LeQuesne, C., Urrutia, R.B., Lara, A., 2012. Multi-century tree-ring based reconstruction of the Neuquén River streamflow, northern Patagonia, Argentina. *Clim. Past* 8, 815–829. <https://doi.org/10.5194/cp-8-815-2012>.
- Muñoz, A.A., González-Reyes, A., Lara, A., Sauchyn, D., Christie, D., Puchi, P., Urrutia-Jalabert, R., Toledo-Guerrero, I., Aguilera-Betti, I., Mundo, I., Sheppard, P.R., Stahle, D., Villalba, R., Szejner, P., LeQuesne, C., Vanstone, J., 2016. Streamflow variability in the Chilean Temperate-Mediterranean climate transition (35°S–42°S) during the last 400 years inferred from tree-ring records. *Clim. Dyn.* 47, 4051–4066. <https://doi.org/10.1007/s00382-016-3068-9>.
- Nasrollahi, N., Aghakouchak, A., Cheng, L., Damberg, L., Phillips, T., Miao, C., Hsu, K., Sorooshian, S., 2015. How well do CMIP5 climate simulations replicate historical trends and patterns of meteorological droughts? *Water Resour. Res.* 51, 2847–2864. <https://doi.org/10.1002/2014WR016318>.
- Opała-Owczarek, M., Niedźwiedź, T., 2018. Last 1100 yr of precipitation variability in western central Asia as revealed by tree-ring data from the Pamir-Alay. *Quat. Res.* 1–15. <https://doi.org/10.1017/qua.2018.21>.
- Orlowsky, B., Seneviratne, S.I., 2013. Elusive drought: uncertainty in observed trends and short- and long-term CMIP5 projections. *Hydrol. Earth Syst. Sci.* 17, 1765–1781. <https://doi.org/10.5194/hess-17-1765-2013>.
- Osborn, T.J., Hulme, M., 1997. Development of a relationship between station and grid-box rainfall frequencies for climate model evaluation. *J. Clim.* 10, 1885–1908. [https://doi.org/10.1175/1520-0442\(1997\)010<1885:DOARBS>2.0.CO;2](https://doi.org/10.1175/1520-0442(1997)010<1885:DOARBS>2.0.CO;2).
- Palmer, W.C., 1965. *Meteorological Drought*. Res. Paper No. 45. U.S. Department of Commerce Weather Bureau, Washington, D.C., p. 58.
- Palmer, J.G., Cook, E.R., Turney, C.S.M., Allen, K., Fenwick, P., Cook, B.I., O'Donnell, A., Lough, J., Grierson, P., Baker, P., 2015. Drought variability in the eastern Australia and New Zealand summer drought atlas (ANZDA, CE 1500–2012). *Environ. Res. Lett.* 10. <https://doi.org/10.1088/1748-9326/10/12/124002>.
- Panyushkina, I.P., Karpukhin, A.A., Engovatova, A.V., 2016. Moisture record of the Upper Volga catchment between AD 1430 and 1600 supported by a $\delta^{13}C$ tree-ring chronology of archaeological pine timbers. *Dendrochronologia* 39, 24–31. <https://doi.org/10.1016/j.dendro.2016.02.002>.
- Pauling, A., Luterbacher, J., Casty, C., Wanner, H., 2006. 500 years of gridded high-resolution precipitation reconstructions over Europe and the connection to large-scale circulation. *Clim. Dyn.* 26, 387–405. <https://doi.org/10.1007/s00382-005-0090-8>.
- Pelletier, J.D., Turcotte, D.L., 1997. Long-range persistence in climatological and hydrological time series: analysis, modeling, and application to drought hazard assessment. *J. Hydrol.* 203, 198–208. [https://doi.org/10.1016/S0022-1694\(97\)00102-9](https://doi.org/10.1016/S0022-1694(97)00102-9).
- Qin, C., Yang, B., Burchardt, I., Hu, X., Kang, X., 2010. Intensified pluvial conditions during the twentieth century in the inland Heihe River Basin in arid north-western China over the past millennium. *Glob. Planet. Chang.* 72, 192–200. <https://doi.org/10.1016/j.gioplacha.2010.04.005>.

- Rossi, S., Deslauriers, A., Anfodillo, T., Carrer, M., 2008. Age-dependent xylogenesis in timberline conifers. *New Phytol.* 177, 199–208. <https://doi.org/10.1111/j.1469-8137.2007.02235.x>.
- Routson, C.C., Woodhouse, C.A., Overpeck, J.T., 2011. Second century megadrought in the Rio Grande headwaters, Colorado: how unusual was medieval drought? *Geophys. Res. Lett.* 38, L22703. <https://doi.org/10.1029/2011GL050015>.
- Rozas, V., DeSoto, L., Olano, J.M., 2009. Sex-specific, age dependent sensitivity of tree-ring growth to climate in the dioecious tree *Juniperus thurifera*. *New Phytol.* 182, 687–697. <https://doi.org/10.1111/j.1469-8137.2009.02770.x>.
- Salzer, M.W., Kipfmüller, K.F., 2005. Reconstructed temperature and precipitation on a millennial timescale from tree-rings in the southern Colorado Plateau, USA. *Clim. Change* 70, 465–487. <https://doi.org/10.1007/s10584-005-5922-3>.
- Saurer, M., Kirdyanov, A.V., Prokushkin, A.S., Rinne, K.T., Siegwolf, R.T.W., 2016. The impact of an inverse climate–isotope relationship in soil water on the oxygen-isotope composition of *Larix gmelinii* in Siberia. *New Phytol.* 209, 955–964. <https://doi.org/10.1111/nph.13759>.
- Schewe, J., Heinke, J., Gerten, D., Haddeland, I., Arnell, N.W., Clark, D.B., Dankers, R., Eisner, S., Fekete, B.M., Colón-González, F.J., Gosling, S.N., Kim, H., Liu, X., Masaki, Y., Portmann, F.T., Satoh, Y., Stacke, T., Tang, Q., Wada, Y., Wisser, D., Albrecht, T., Frieler, K., Piontek, F., Warszawski, L., Kabat, P., 2014. Multimodel assessment of water scarcity under climate change. *Proc. Natl. Acad. Sci. Unit. States Am.* 111, 3245–3250. <https://doi.org/10.1073/pnas.1222460110>.
- Schneider, L., Ljungqvist, F.C., Yang, B., Chen, F., Chen, J., Li, J., Hao, Z., Ge, Q., Talento, S., Osborn, T.J., Luterbacher, J., 2019. The impact of proxy selection strategies on a millennium long ensemble of hydroclimatic records in Monsoon Asia. *Quat. Sci. Rev.* 223, 105917. <https://doi.org/10.1016/j.quascirev.2019.105917>.
- Schulman, E., 1945. *Tree-ring Hydrology of the Colorado River Basin*, vol. 14. University of Arizona Bulletin Series, p. 51. LTRR Bulletin No. 2.
- Schulman, E., 1956. *Dendroclimatic Changes in Semiarid America*. University of Arizona Press, Tucson.
- Schweingruber, F., 1988. *Tree Rings: Basics and Applications of Dendrochronology*. Reidel, Dordrecht.
- Seftigen, K., Björklund, J., Cook, E.R., Linderholm, H.W., 2015a. A tree-ring field reconstruction of Fennoscandian summer hydroclimate variability for the last millennium. *Clim. Dyn.* 44, 3141–3154. <https://doi.org/10.1007/s00382-014-2191-8>.
- Seftigen, K., Cook, E., Linderholm, H., Fuentes, M., Björklund, J., 2015b. The potential of deriving tree-ring-based field reconstructions of droughts and pluvials over Fennoscandia. *J. Clim.* 28, 3453–3471. <https://doi.org/10.1175/JCLI-D-13-00734.1>.
- Seftigen, K., Goosse, H., Klein, F., Chen, D., 2017. Hydroclimatic variability in Scandinavia over the last millennium – insights from a climate model–proxy data comparison. *Clim. Past* 13, 1831–1850. <https://doi.org/10.5194/cp-13-1831-2017>.
- Seftigen, K., Frank, D.C., Björklund, J., Babst, F., Poulter, B., 2018. The climatic drivers of normalized difference vegetation index and tree-ring-based estimates of forest productivity are spatially coherent but temporally decoupled in Northern Hemispheric forests. *Glob. Ecol. Biogeogr.* 27, 1352–1365. <https://doi.org/10.1111/geb.12802>.
- Seim, A., Tulyaganov, T., Omurova, G., Nikolyai, L., Botman, E., Linderholm, H.W., 2016a. Dendroclimatological potential of three juniper species from the Turkestan range, northwestern Pamir–Alay Mountains. *Uzbekistan. Trees* 30, 733–748. <https://doi.org/10.1007/s00468-015-1316-y>.
- Seim, A., Omurova, G., Azisov, E., Musuraliev, K., Aliev, K., Tulyaganov, T., Nikolyai, L., Botman, E., Helle, G., Dorado Liñan, I., Jivcov, S., Linderholm, H.W., 2016b. Climate change increases drought stress of juniper trees in the Mountains of Central Asia. *PLoS One* 11, e0153888. <https://doi.org/10.1371/journal.pone.0153888>.
- Shah, S.K., Touchan, R., Babushkina, E., Shishov, V.V., Meko, D.M., Abramenko, O.V., Belokopytova, L.V., Hordo, M., Jevšenak, J., Kędziora, W., Kostyakova, T.V., Moskwa, A., Oleksiak, Z., Omurova, G., Ovchinnikov, S., Sadeghpour, M., Saikia, A., Zsewastynowicz, L., Sidenko, T., Strantsov, A., Tamkevičiūtė, M., Tomusiak, R., Tychkov, I., 2015. August to July precipitation from tree rings in the forest-steppe zone of Central Siberia (Russia). *Tree-Ring Res.* 71, 37–44. <https://doi.org/10.3959/1536-1098-71.1.37>.
- Shao, X.M., Huang, L., Liu, H.B., Liang, E.Y., Fang, X.Q., Wang, L.L., 2005. Reconstruction of precipitation variation from tree rings in recent 1000 years in Delingha, Qinghai. *Sci. China Earth Sci.* 48, 939–949. <https://doi.org/10.1360/03yd0146>.
- Sheppard, P., Tarasov, P.E., Graumlich, L., Heussner, K.-U., Wagner, M., Österle, H., Thompson, L., 2004. Annual precipitation since 515 BC reconstructed from living and fossil juniper growth of northeastern Qinghai Province, China. *Clim. Dyn.* 23, 869–881. <https://doi.org/10.1007/s00382-004-0473-2>.
- Shestakova, T.A., Voltas, J., Saurer, M., Siegwolf, R.T.W., Kirdyanov, A.V., 2017. Warming effects on *Pinus sylvestris* in the cold–dry Siberian forest–steppe: positive or negative balance of trade? *Forests* 8, 490. <https://doi.org/10.3390/f8120490>.
- Shestakova, T.A., Gutiérrez, E., Valeriano, C., Lapshina, E., Voltas, J., 2019. Recent loss of sensitivity to summer temperature constrains tree growth synchrony among boreal Eurasian forests. *Agric. For. Meteorol.* 268, 318–330. <https://doi.org/10.1016/j.agrformet.2019.01.039>.
- Sidorova, O.V., Naurzbaev, M.M., Vaganov, E.A., 2006. An integral estimation of tree-ring chronologies from subarctic regions of Eurasia. *Trace* 4, 84–91.
- Sidorova, O.V., Siegwolf, R.T.W., Saurer, M., Shashkin, A.V., Knorre, A.A., Prokushkin, A.S., Kirdyanov, A.V., 2009. Do centennial tree-ring and stable isotope trends of *Larix gmelinii* (Rupr.) Rupr. indicate increasing water shortage in the Siberian north? *Oecologia* 161, 825–835. <https://doi.org/10.1007/s00442-009-1411-0>.
- Sidorova, O.V., Siegwolf, R.T.W., Saurer, M., Naurzbaev, M.M., Shashkin, A.V., Vaganov, E.A., 2010. Spatial patterns of climatic changes in the Eurasian north reflected in Siberian larch tree-ring parameters and stable isotopes. *Glob. Chang. Biol.* 16, 1003–1018. <https://doi.org/10.1111/j.1365-2486.2009.02008.x>.
- Sidorova, O.V., Saurer, M., Myglan, V.S., Eichler, A., Schwikowski, M., Kirdyanov, A.V., Bryukhanova, M.V., Gerasimova, O.V., Kalugin, I.A., Daryin, A.V., Siegwolf, R.T.W., 2012. A multi-proxy approach for revealing recent climatic changes in the Russian Altai. *Clim. Dyn.* 38, 175–188. <https://doi.org/10.1007/s00382-010-0989-6>.
- Smerdon, J.E., Pollack, H.N., 2016. Reconstructing Earth's surface temperature over the past 2000 years: the science behind the headlines. *Wiley Interdiscip. Rev. Clim. Change* 7, 746–771. <https://doi.org/10.1002/wcc.418>.
- Smerdon, J.E., Cook, B.I., Cook, E.R., Seager, R., 2015. Bridging past and future climate across paleoclimatic reconstructions, observations, and models: a hydroclimate case study. *J. Clim.* 28, 3212–3231. <https://doi.org/10.1175/JCLI-D-14-00417.1>.
- Solomina, O., Maximova, O., Cook, E., 2014. *Picea schrenkiana* ring width and density at the upper and lower tree limits in the Tien Shan Mts (Kyrgyz Republic) as a source of paleoclimatic information. *Geogr., Environ., Sustain.* 7, 66–79. <https://doi.org/10.24057/2071-9388-2014-7-1-66-79>.
- Solomina, O.N., Bushueva, I.S., Dolgova, E.A., Zolotokrylin, A.N., Kuznetsova, V.V., Kuznetsova, T.O., Kuhta, A.E., Lazukova, L.I., Lomakin, N.A., Matkovsky, V.V., Matveev, S.M., Mikhailov, A.Y., Mikhailenko, V.N., Pojdaeva, D.S., Rumyantsev, D.E., Sakulina, G.A., Semenov, V.A., Khasanov, B.F., Tcherenkova, E.A., Tchernokulsky, A.V., 2017. Droughts of the East European Plain According to Hydrometeorological and Tree-Ring Data. Nestor-Historia, Moscow, Saint Petersburg [in Russian].
- Speer, J.H., 2010. *Fundamentals of Tree-Ring Research*. University of Arizona Press, Tucson.
- St George, S., 2014. An overview of tree-ring width records across the Northern Hemisphere. *Quat. Sci. Rev.* 95, 132–150. <https://doi.org/10.1016/j.quascirev.2014.04.029>.
- St George, S., Ault, T.R., 2014. The imprint of climate within Northern Hemisphere trees. *Quat. Sci. Rev.* 89, 1–4. <https://doi.org/10.1016/j.quascirev.2014.01.007>.
- Stahle, D.W., Cleaveland, M.K., 1992. Reconstruction and analysis of spring rainfall over the Southeastern U.S. for the past 1000 years. *Bull. Am. Meteorol. Soc.* 73, 1947–1961. [https://doi.org/10.1175/1520-0477\(1992\)073<1947:RAOSR>2.0.CO;2](https://doi.org/10.1175/1520-0477(1992)073<1947:RAOSR>2.0.CO;2).
- Stahle, D.W., Cleaveland, M.K., Grissino-Mayer, H., Griffin, R.D., Fye, F.K., Therrell, M.D., Burnette, D.J., Meko, D.M., Villanueva Diaz, J., 2009. Cool and warm season precipitation reconstructions over western New Mexico. *J. Clim.* 22, 3729–3750. <https://doi.org/10.1175/2008JCLI2752.1>.
- Stahle, D.W., Diaz, J.V., Burnette, D.J., Paredes, J.C., Heim, R.R., Fye, F.K., Soto, R.A., Therrell, M.D., Cleaveland, M.K., Stahle, D.K., 2011. Major Mesoamerican droughts of the past millennium. *Geophys. Res. Lett.* 38, L05703. <https://doi.org/10.1029/2010GL046472>.
- Stahle, D.W., Burnette, D.J., Villanueva, J., Cerano, J., Fye, F.K., Griffin, R.D., Cleaveland, M.K., Stahle, D.K., Edmondson, J.R., Wolff, K.P., 2012. Tree-ring analysis of ancient baldcypress trees and subfossil wood. *Quat. Sci. Rev.* 34, 1–15. <https://doi.org/10.1016/j.quascirev.2011.11.005>.
- Stahle, D.K., Burnette, D.J., Stahle, D.W., 2013. A moisture balance reconstruction for the drainage basin of Albemarle Sound, North Carolina. *Estuar. Coasts* 36, 1340–1353. <https://doi.org/10.1007/s12237-013-9643-y>.
- Stahle, D.W., Edmondson, J.R., Burns, J.N., Stahle, D.K., Burnette, D.J., Kvamme, E., Lequesne, C., Therrell, M.D., 2015. Bridging the gap with subfossil Douglas-Fir at Mesa Verde, Colorado. *Tree-Ring Res.* 71, 53–66. <https://doi.org/10.3959/1536-1098-71.2.53>.
- Stahle, D.W., Cook, E.R., Burnette, D.J., Villanueva, J., Cerano, J., Burns, J.N., Griffin, D., Cook, B.I., Acuña, R., Torbenson, M.A.C., Szejner, P., Howard, I.M., 2016. The Mexican Drought Atlas: Tree-ring reconstructions of the soil moisture balance during the late pre-Hispanic, colonial, and modern eras. *Quat. Sci. Rev.* 149, 34–60. <https://doi.org/10.1016/j.quascirev.2016.06.018>.
- Stambaugh, M.C., Guyette, R.P., McMurtry, E.R., Cook, E.R., Meko, D.M., Lupo, A.R., 2011. Drought duration and frequency in the US Corn Belt during the last millennium (AD 992–2004). *Agric. For. Meteorol.* 151, 154–162. <https://doi.org/10.1016/j.agrformet.2010.09.010>.
- Stephens, G.L., L'Ecuier, T., Forbes, R., Gettleman, A., Golaz, J.-C., Bodas-Salcedo, A., Suzuki, K., Gabriel, P., Haynes, J., 2010. Dreary state of precipitation in global models. *J. Geophys. Res.* 115, D24211. <https://doi.org/10.1029/2010JD014532>.
- Stockton, C.W., 1975. *Long-term Streamflow Records Reconstructed from Tree-Rings*. University of Arizona Press, Tucson, p. 111.
- Stockton, C.W., Jacoby, G.C., 1976. Long-term surface-water supply and streamflow trends in the Upper Colorado River Basin based on tree-ring analysis. *Lake Powell Res. Proj. Bull.* 18, 1–70.
- Stokes, M.A., Smiley, T.L., 1968. *An Introduction to Tree-Ring Dating*. University of Chicago Press, Chicago, p. 110.
- Sugimoto, A., Yanagisawa, N., Naito, D., Fujita, N., Maximov, T.C., 2002. Importance of permafrost as a source of water for plants in east Siberian taiga. *Ecol. Res.* 17, 493–503. <https://doi.org/10.1046/j.1440-1703.2002.00506.x>.
- Tegel, W., Vanmoerkerke, J., Büntgen, U., 2010. Updating historical tree-ring records for climate reconstruction. *Quat. Sci. Rev.* 29, 1957–1959. <https://doi.org/10.1016/j.quascirev.2010.05.018>.
- Tei, S., Sugimoto, A., Yonenobu, H., Yamazaki, T., Maximov, T.C., 2013. Reconstruction of soil moisture for the past 100 years in eastern Siberia by using $\delta^{13}\text{C}$ of larch

- tree rings. *J. Geophys. Res.: Biogeosciences* 118, 1256–1265. <https://doi.org/10.1002/jgrg.20110>.
- Tei, S., Yonenobu, H., Sugimoto, A., Ohta, T., Maximov, T.C., 2015. Reconstructed summer Palmer Drought Severity Index since 1850 AD based on $\delta^{13}\text{C}$ of larch tree rings in eastern Siberia. *J. Hydrol.* 529, 442–448. <https://doi.org/10.1016/j.jhydrol.2015.01.085>.
- Thomsen, G., 2001. Response to winter precipitation in ring-width chronologies of *Pinus sylvestris* L. from the northwestern Siberian plain, Russia. *Tree-Ring Res.* 57, 15–29.
- Touchan, R., Meko, D., Hughes, M.K., 1999. A 396-year reconstruction of precipitation in southern Jordan. *J. Am. Water Resour. Assoc.* 5, 49–59. <https://doi.org/10.1111/j.1752-1688.1999.tb05451.x>.
- Touchan, R., Garfin, G.M., Meko, D., Funkhouser, G., Erkan, N., Hughes, M.K., Wallin, B.S., 2003. Preliminary reconstructions of spring precipitation in southwestern Turkey from tree-ring width. *Int. J. Climatol.* 23, 157–171. <https://doi.org/10.1002/joc.850>.
- Touchan, R., Funkhouser, G., Hughes, M.K., Erkan, N., 2005. Standardized precipitation index reconstructed from Turkish tree-ring widths. *Clim. Change* 72, 339–353. <https://doi.org/10.1007/s10584-005-5358-9>.
- Touchan, R., Akkemik, Ü., Hughes, M.K., Erkan, N., 2007. May–June precipitation reconstruction of southwestern Anatolia, Turkey during the last 900 years from tree rings. *Quat. Res.* 68, 196–202. <https://doi.org/10.1016/j.yqres.2007.07.001>.
- Touchan, R., Woodhouse, C., Meko, D., Allen, C., 2011. Millennial precipitation reconstruction for the Jemez mountains, New Mexico, reveals changing drought signal. *Int. J. Climatol.* 31, 896–906. <https://doi.org/10.1002/joc.2117>.
- Treydte, K.S., Schleser, G.H., Helle, G., Frank, D.C., Winiger, M., Haug, G.H., Esper, J., 2006. The twentieth century was the wettest period in northern Pakistan over the past millennium. *Nature* 440, 1179–1182. <https://doi.org/10.1038/nature04743>.
- Trnka, M., Hayes, M., Jurečka, F., Bartošová, L., Anderson, M., Brázdil, R., Brown, J., Camarero, J.J., Cudlín, P., Dobrovolný, P., Eitzinger, J., Feng, S., Finnessey, T., Gregorič, G., Havlik, P., Hain, C., Holman, I., Johnson, D., Kersebaum, K.C., Ljungqvist, F.C., Luterbacher, J., Micale, F., Hartl-Meier, C., Možný, M., Nejedlik, P., Olesen, J.E., Ruiz-Ramos, M., Rötter, R.P., Senay, G., Serrano, S.M.V., Svoboda, M., Susnik, A., Tadesse, T., Vizina, A., Wardlaw, B., Žalud, Z., Büntgen, U., 2018. Priority questions in multidisciplinary drought research. *Clim. Res.* 75, 241–260. <https://doi.org/10.3354/cr01509>.
- Urrutia, R.B., Lara, A., Villalba, R., Christie, D.A., Le Quesne, C., Cuq, A., 2011. Multi-century tree ring reconstruction of annual streamflow for the Maule River watershed in south central Chile. *Water Resour. Res.* 47, W06527. <https://doi.org/10.1029/2010WR009562>.
- van der Schrier, G., Jones, P.D., Briffa, K.R., 2011. The sensitivity of the PDSI to the Thornthwaite and Penman–Monteith parameterizations for potential evapotranspiration. *J. Geophys. Res.* 116, D03106. <https://doi.org/10.1029/2010JD015001>.
- Wan, H., Zhang, X., Zwiers, F.W., Shiogama, H., 2013. Effect of data coverage on the estimation of mean and variability of precipitation at global and regional scales. *J. Geophys. Res. Atmos.* 118, 534–546. <https://doi.org/10.1002/jgrd.50118>.
- Wang, W., Liu, X., Xu, G., Shao, X., Qin, D., Sun, W., An, W., Zeng, X., 2013. Moisture variations over the past millennium characterized by Qaidam Basin tree-ring $\delta^{18}\text{O}$. *Sci. Bull.* 58, 3956–3961. <https://doi.org/10.1007/s11434-013-5913-0>.
- Wang, H.Q., Chen, F., Ermenbaev, B., Satylkanov, R., 2017. Comparison of drought-sensitive tree-ring records from the Tien Shan of Kyrgyzstan and Xinjiang (China) during the last six centuries. *Adv. Clim. Change Res.* 8, 18–25. <https://doi.org/10.1016/j.accre.2017.03.004>.
- Waterhouse, J.S., Barker, A.C., Carter, A.H.C., Agafonov, L.I., Loader, N.J., 2000. Stable carbon isotopes in Scots pine tree rings preserve a record of flow of the river Ob. *Geophys. Res. Lett.* 27, 3529–3532. <https://doi.org/10.1029/2000GL006106>.
- Wells, N., Goddard, S., Hayes, M.J., 2004. A self-calibrating Palmer Drought Severity Index. *J. Clim.* 17, 2335–2351. [https://doi.org/10.1175/1520-0442\(2004\)017<2335:ASPDST>2.0.CO;2](https://doi.org/10.1175/1520-0442(2004)017<2335:ASPDST>2.0.CO;2).
- Wigley, T.M.L., Briffa, K.R., Jones, P.D., 1984. On the average of correlated time series, with applications in dendroclimatology and hydrometeorology. *J. Clim. Appl. Meteorol.* 23, 201–213. [https://doi.org/10.1175/1520-0450\(1984\)023<0201:OTAVOC>2.0.CO;2](https://doi.org/10.1175/1520-0450(1984)023<0201:OTAVOC>2.0.CO;2).
- Wilson, R., Miles, D., Loader, N.J., Melvin, T., Cunningham, L., Cooper, R., Briffa, K., 2013. A millennial long March–July precipitation reconstruction for southern-central England. *Clim. Dyn.* 40, 997–1017. <https://doi.org/10.1007/s00382-012-1318-z>.
- Woodhouse, C.A., Gray, S.T., Meko, D.M., 2006. Updated streamflow reconstructions for the upper Colorado River Basin. *Water Resour. Res.* 42, W05415. <https://doi.org/10.1029/2005WR004455>.
- Woodhouse, C.A., Pederson, G.T., Gray, S.T., 2011. An 1800-yr record of decadal-scale hydroclimatic variability in the upper Arkansas River basin from bristlecone pine. *Quat. Res.* 75, 483–490. <https://doi.org/10.1016/j.yqres.2010.12.007>.
- Xoplaki, E., Fleitmann, D., Luterbacher, J., Wagner, S., Haldon, J.F., Zorita, E., Telis, I., Toreti, A., Izdebski, A., 2016. The Medieval Climate Anomaly and Byzantium: a review of the evidence on climatic fluctuations, economic performance and societal change. *Quat. Sci. Rev.* 136, 229–252. <https://doi.org/10.1016/j.quascirev.2015.10.004>.
- Xoplaki, E., Luterbacher, J., Wagner, S., Zorita, E., Fleitmann, D., Preiser-Kapeller, J., Sargent, A.M., White, S., Toreti, A., Haldon, J.F., Mordechai, L., Bozkurt, D., Akçer-Ön, S., Izdebski, A., 2018. Modelling climate and societal resilience in the Eastern Mediterranean in the last millennium. *Hum. Ecol.* 46, 363–379. <https://doi.org/10.1007/s10745-018-9995-9>.
- Yang, B., Qin, C., Shi, F., Sonechkin, D.M., 2012. Tree ring-based annual streamflow reconstruction for the Heihe River in arid northwestern China from AD 575 and its implications for water resource management. *Holocene* 22, 773–784. <https://doi.org/10.1177/0959683611430411>.
- Yang, B., Qin, C., Wang, J., He, M., Melvin, T.M., Osborn, T.J., Briffa, K.R., 2014. A 3,500-year tree-ring record of annual precipitation on the northeastern Tibetan Plateau. *Proc. Natl. Acad. Sci. Unit. States Am.* 111, 2903–2908. <https://doi.org/10.1073/pnas.1319238111>.
- Yang, B., Wang, J., Liu, J., 2019. A 1556-year-length early summer moisture reconstruction for the Hexi Corridor, Northwestern China. *Sci. China Earth Sci.* 62, 953–963. <https://doi.org/10.1007/s11430-018-9327-1>.
- Yin, Z.Y., Shao, X.M., Qin, N.S., Liang, E.Y., 2008. Reconstruction of a 1436-year soil moisture and vegetation water use history based on tree-ring widths from Qilian junipers in northeastern Qaidam Basin, northwestern China. *Int. J. Climatol.* 28, 37–53. <https://doi.org/10.1002/joc.1515>.
- Zhang, Y., Tian, Q., Gou, X., Chen, F., Leavitt, S.W., Wang, Y., 2011. Annual precipitation reconstruction since AD 775 based on tree rings from the Qilian Mountains, northwestern China. *Int. J. Climatol.* 31, 371–381. <https://doi.org/10.1002/joc.2085>.
- Zhang, H., Yuan, N., Xoplaki, E., Werner, J., Büntgen, U., Esper, J., Treydte, K., Luterbacher, J., 2015. Modified climate with long term memory in tree ring proxies. *Environ. Res. Lett.* 10, 084020. <https://doi.org/10.1088/1748-9326/10/8/084020>.
- Zhang, R., Shang, H., Yu, S., He, Q., Yuan, Y., Bolatov, K., Mambetov, B.T., 2017. Tree-ring-based precipitation reconstruction in southern Kazakhstan, reveals drought variability since AD 1770. *Int. J. Climatol.* 37, 741–750. <https://doi.org/10.1002/joc.4736>.